DAMAGE THRESHOLD STUDIES IN LASER CRYSTALS:
BEAM INTENSITY PROFILE AND SELF-FOCUSING

By
Concetto R. Giuliano
Donald F. DuBois
Robert W. Hellwarth
Gerald R. Rickel

HUGHES RESEARCH LABORATORIES
HUGHES AIRCRAFT COMPANY
3011 Malibu Canyon Road
Malibu, California 90265

Contract NO. F19628-69-C-0277
Project NO. 8693

SEMIANNUAL REPORT NO.3
JANUARY 1971

Contract Monitor: C. Martin Stickley
OPTICAL PHYSICS LABORATORY

Sponsored by
Advanced Research Projects Agency
ARPA Order No. 1434
Monitored by
AIR FORCE CAMBRIDGE RESEARCH LABORATORIES
AIR FORCE SYSTEMS COMMAND
UNITED STATES AIR FORCE
BEDFORD, MASSACHUSETTS 01730

70

AFCRL-71-0064

DAMAGE THRESHOLD STUDIES IN LASER CRYSTALS: BEAM INTENSITY PROFILE AND SELF-FOCUSING

By

Concetto R. Giuliano, Donald F. DuBois,
Robert W. Hellwarth and Gerald R. Rickel

HUGHES RESEARCH LABORATORIES
Malibu, California 90265
A Division of Hughes Aircraft Company

Contract No. F19628-69-C-0277
Project No. 8693

Semiannual Report No. 3
January 1971

Contract Monitor: C. Martin Stickley
Optical Physics Laboratory

Sponsored by
Advanced Research Projects Agency
ARPA Order No. 1434

Monitored by
AIR FORCE CAMBRIDGE RESEARCH LABORATORIES
AIR FORCE SYSTEMS COMMAND
UNITED STATES AIR FORCE
BEDFORD, MASSACHUSETTS 01730

Program Code No. 0D10

Effective Date of Contract....21 May 1969

Contract Expiration Date.....15 July 1971

Principal Investigator and
Phone No. .....Concetto R. Giuliano/213 456-6411 Ext 285

Project Scientist or Engineer
and Phone No. .....C. Martin Stickley/617 861-2694

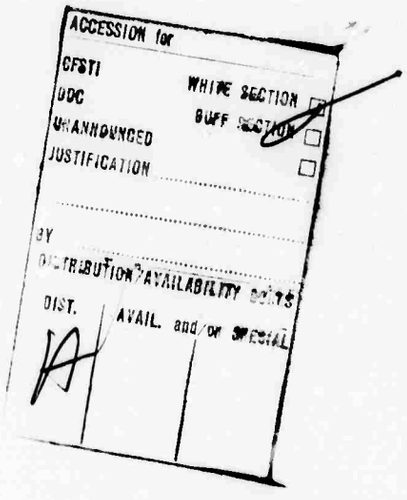

Qualified requestors may obtain additional copies from the Defense Documentation Center. All others should apply to the National Technical Information Service.

ABSTRACT

In this report the results of a number of experiments are presented which were aimed at detailed characterization of the spatial profile of the laser beam both before and after amplification. It was found that the beam profile in the near field of the laser deviates significantly from a gaussian, but that in the far field it is very close to a gaussian. It was also found that while the amplifier does not contribute to significant beam distortion, it acts as a negative lens whose focal length decreases with increased optical pumping. The purpose of these continuing measurements is to have a close measurement of the size and location of the focused beam waist. Based on these measurements, revised values of previous damage thresholds are presented as well as the results of measurements of damage threshold as a function of lens focal length. In other experiments, the time evolution of the damage tracks in ruby and sapphire was studied using a fast streaking camera. It was found that the point on the damage filament furthest from the laser forms first, and the track evolves in an upstream direction. Beam profile measurements inside ruby samples show a severe power dependent beam distortion which begins to appear at powers well below the damage threshold. This breaking up of the beam is not observed in sapphire. It is possible that this breaking up of the beam in ruby is connected with the absorption at 6943 Å. Because of the importance of self-focusing considerations in damage studies, a detailed derivation of theoretical results reported recently by other workers is presented as an appendix.

TABLE OF CONTENTS

LIST OF ILLUSTRATIONS

SECTION I

EXPERIMENTAL STUDIES ON OPTICAL DAMAGE

A. INTRODUCTION AND SUMMARY OF RESULTS

During this period we have carried out a number of measurements aimed at characterizing our laser beam profile, both before and after amplification. The purpose of these measurements is to determine more precisely the size and location of the focused spot, as well as the beam shape, so that more accurate energy density measurements can be obtained. We have found that the beam profile is approximately gaussian in the far field of the oscillator, but that in the near field an appreciable deviation from gaussian behavior exists. We have also found that the amplifier acts as a negative lens appreciably increasing the beam divergence of the oscillator to up to a factor of 2 for the most intense pumping studied. This results in an appreciable shift in the beam waist for the longer focal length lenses used in the early damage threshold experiments. Revised threshold data are presented based on the beam profile measurements.

A most significant result was obtained when beam profile measurements were made in ruby. We found a radical power dependent departure from the smooth profile indicating a severe breaking up of the beam. This radical beam distortion raises doubts as to the possibility of measuring power density for ruby. The effect, which for ruby is seen to appear at least an order of magnitude below the bulk damage threshold, is not seen in sapphire all the way up to and beyond the bulk damage threshold.

We also present in this report the results of some early damage threshold experiments in ruby measured with lenses of different focal length. In addition, we present high speed streak camera pictures which show that the damage track begins to form at a point furthest from the source and then moves upstream toward the laser.

B. BEAM PROFILE MEASUREMENTS AND COMPARISON WITH GAUSSIAN DISTRIBUTION

All of the damage threshold power densities in previous reports were based on beam sizes calculated according to the following assumptions:

- The spatial beam profile at the laser output mirror is gaussian with a 1 mm radius (1/e radius for the electric field).
- The beam diffracts according to the well-known expressions for gaussian beam propagation.
- The beam suffers no distortion, focusing, or defocusing on passing through the ruby amplifier and hence the diffraction-limited beam waist occurs at the location calculated according to the propagation equations.

During this period we have looked more carefully into the validity of these assumptions and will discuss the results in this report.

The apparatus used in the experiments carried out in this period is essentially the same as that described in previous Semiannual Reports Nos. 1 and 2. Figure 1 shows a schematic representation of the laser, amplifier, and associated monitoring apparatus used in the studies. The apparatus described briefly consists of a mode controlled ruby laser Q-switched with a cryptocyanine solution. Both oscillator and amplifier are operated at 0°C. The combined effect of the temperature controlled resonant reflector and the dye allow the laser to operate in a single longitudinal mode and the aperture allows a single transverse mode.

Monitoring equipment enables the shot-to-shot measurement of near field, far field, and Fabry-Perot patterns of the oscillator as well as power output measurements of the oscillator before and after amplification. A more detailed description of this apparatus is available from previous reports.

In order to test the validity of the above assumptions, we have undertaken a series of measurements to determine the spatial beam

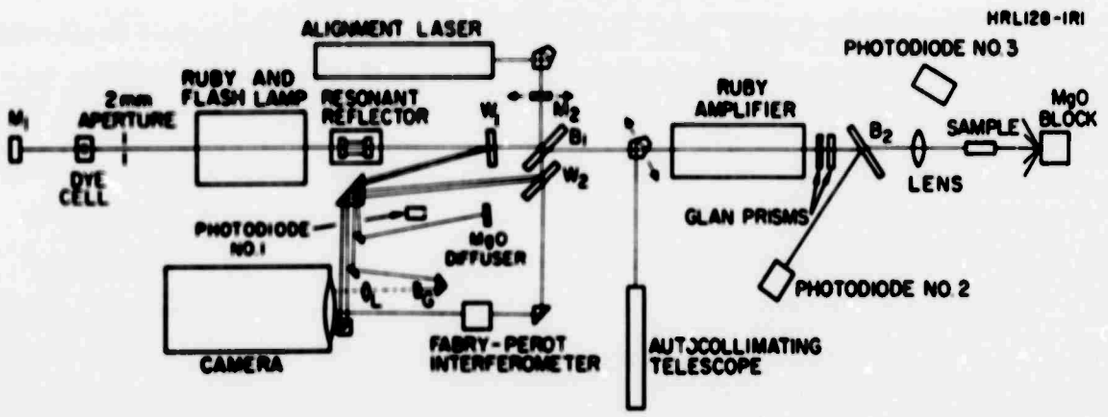

Fig. 1. Schematic Representation of Experimental Apparatus used in Damage Threshold Measurements.

profile at different locations and under a number of different conditions. Early experiments employed the measurement of a pair of spots with a known relative attenuation for both near and far field spot sizes. As mentioned in the previous report, we obtained a near field spot size of 1 mm (~15 percent accuracy) by photographing a pair of spots on a ground glass screen and also by measuring beam patterns on exposed Polaroid film with the relative energies of successive shots known. Far field divergence measurements of the unamplified oscillator using the two spot technique gave a divergence of 0.3 ±0.05 mrad (half-angle). These results are based on the assumption that the beam profile is gaussian.

During this period we have attempted to determine how close to gaussian the beam profile actually is. To accomplish this we have used a multiple lens camera and the technique described by Winer[1]. The setup is described in Fig. 2. We image a particular plane (plane A) onto a MgO block with the imaging lens choosing the object and image distances to get convenient magnification, and photograph the spot on the MgO block with the multiple lens camera. (This is accomplished by placing a pinhole of known size at plane A, imaging it on the MgO block with appropriate magnification, and photographing it.) The camera has nine lenses (f = ~11 cm, 12 mm diameter) each of which is backed by a different calibrated neutral density (N. D.) filter. Thus we obtain nine spots on the focal plane of the camera with known relative exposures. The first few measurements were made with density steps of 0.1 between successive lenses, giving us a total span of over a factor of 6 from the first (N. D. 0) to the last (N. D. 0.8) lens in the array. We later chose a different set of densities to give a greater total span (a factor of 12.6). These are N. D. 0, 0.2, 0.4, 0.6, 0.7, 0.8, 0.9, 1.0, and 1.1.

The principle of the multiple lens camera technique for measuring intensity profiles is that the film response need not be known. Densitometer scans of the different spots are made, and the widths of the scans are measured at a constant density determined by the peak of the curve with the least transmission (see Fig. 3). The image filter transmission ratios (T_1/T_n) are plotted against the corresponding widths (d_n) giving the spatial intensity profile. Examples are shown in Figs. 5 to 8.

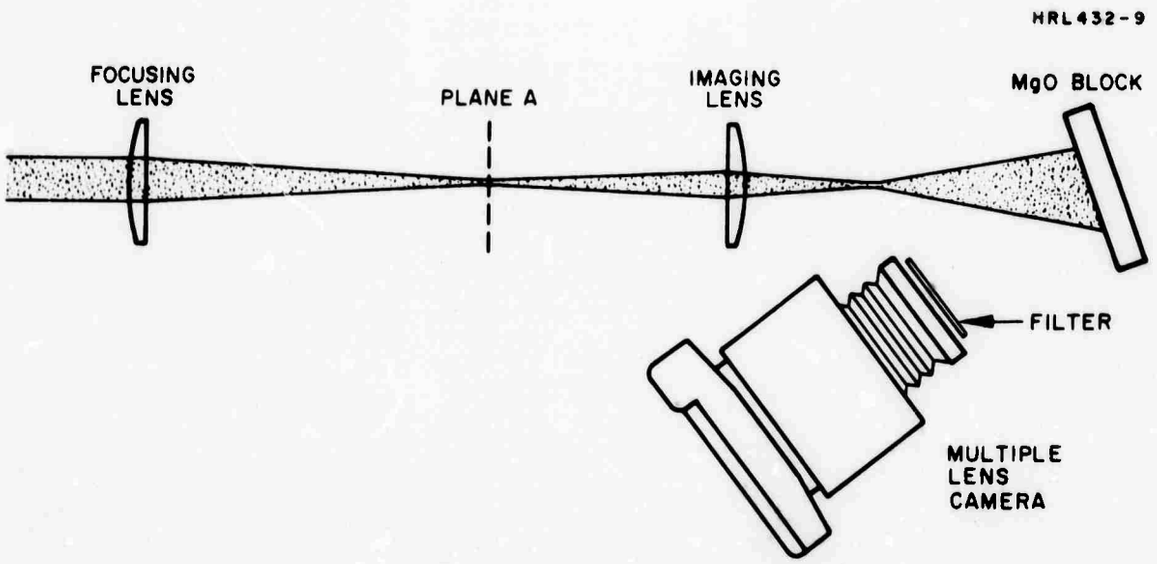

Fig. 2. Schematic Representation of Setup Used in Beam Profile Measurements.

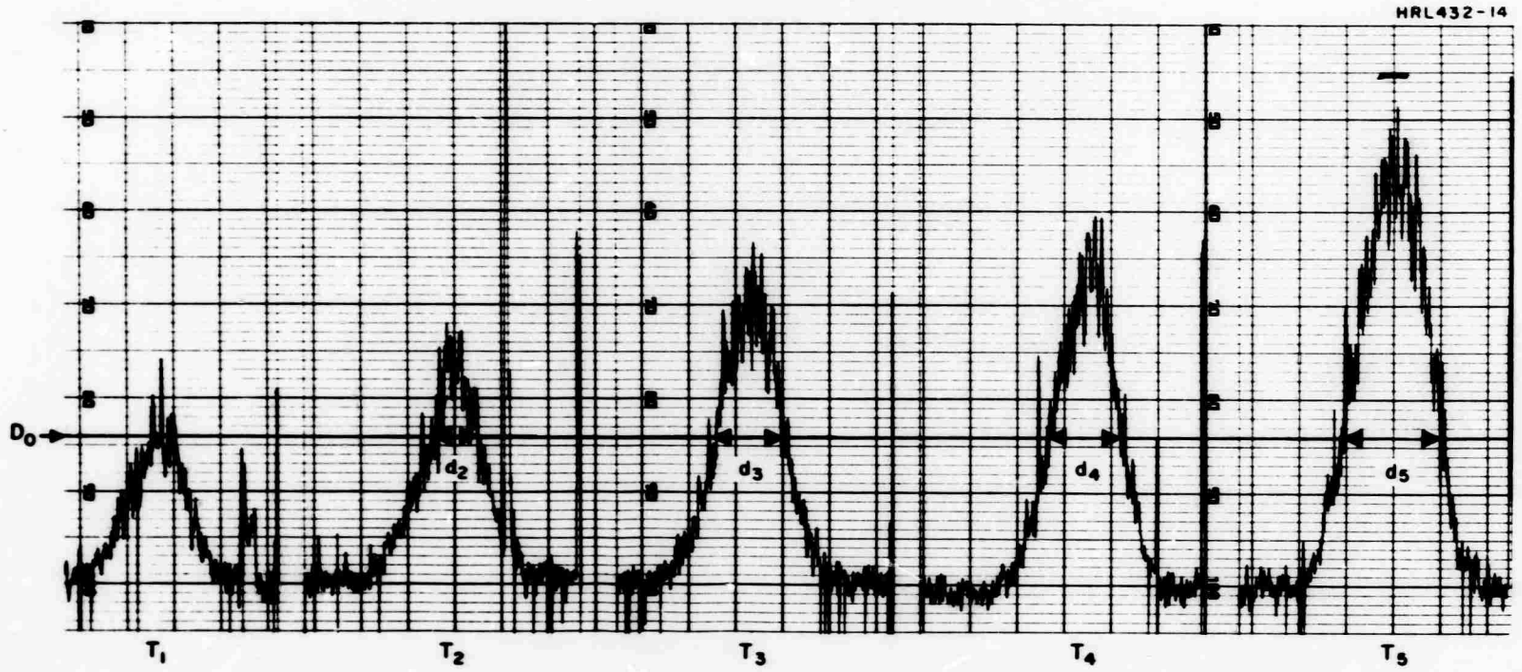

Fig. 3. Example of Microdensitometer Scans for a Typical Plate Shown in Fig. 4. (Five of the nine scans are shown). The Widths d_n at Constant Density D_0 are Plotted Against the Relative Filter Transmission Ratios T_1/T_n to Give Spatial Distributions as Seen in Figs. 5 through 8.

During this investigation we have used a number of different recording media. At first Polaroid Type 55 P/N film was used, but was found to be too low in sensitivity. Other measurements were made with Kodak Type I-N and IV-N spectroscopic plates. (The IV-N plates have a much smaller dynamic range than the I-N being about 15 times more sensitive. Also the graininess is higher, giving rise to even more noise in the densitometer scans than the already noisy I-N densitometer scans.) The plates were scanned with a Jarrel-Ash microdensitometer at rates ranging from 1 to 2.5 mm/min. A typical plate is shown in Fig. 4.

Beam cross-sections were photographed at different places and under different conditions of pumping the amplifier. For example, we measured the beam size at the output resonant reflector of the oscillator at the exit of the amplifier, at the focusing lens position, and at various locations beyond the focusing lens, including the focal plane.

Comparison of Densitometer Scans with Gaussians – The data obtained from the densitometer scans were fed into a computer, programmed to give it the best fit to a gaussian based on a least-squares calculation. The fit to a gaussian was fairly good, depending upon the region in space examined. A number of these plots are shown in Figs. 5 to 8. We see from these figures that there is a fair amount of data scatter from the calculated best gaussian fit, but that the agreement is fairly good. The largest deviation from gaussian behavior appears to be at the output mirror of the laser (Fig. 5), where we see the intensity in the wings dropping much faster than that in the calculated curves. This truncation is not so evident as the beam propagates away from the laser into the far field. (Figures 6 to 8.) We also notice a fair amount of scatter in the experimental points from shot to shot. This could arise from small differences in alignment, both of oscillator and amplifier, from shot to shot or from scatter in the measurements taken from the densitometer scans. As we see in Fig. 3, the location of the maximum, D_o, for the reference scan (i.e., the one corresponding to least exposure on the plate) determines the values of widths taken from the successive

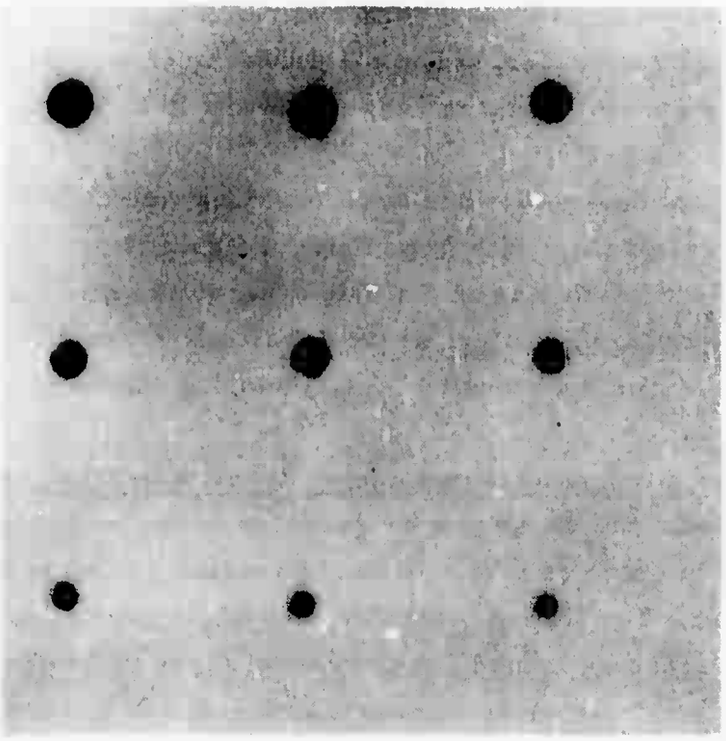

Fig. 4. A Typical Spectrographic Plate Showing Multiple Exposures of Laser Beam Profile.

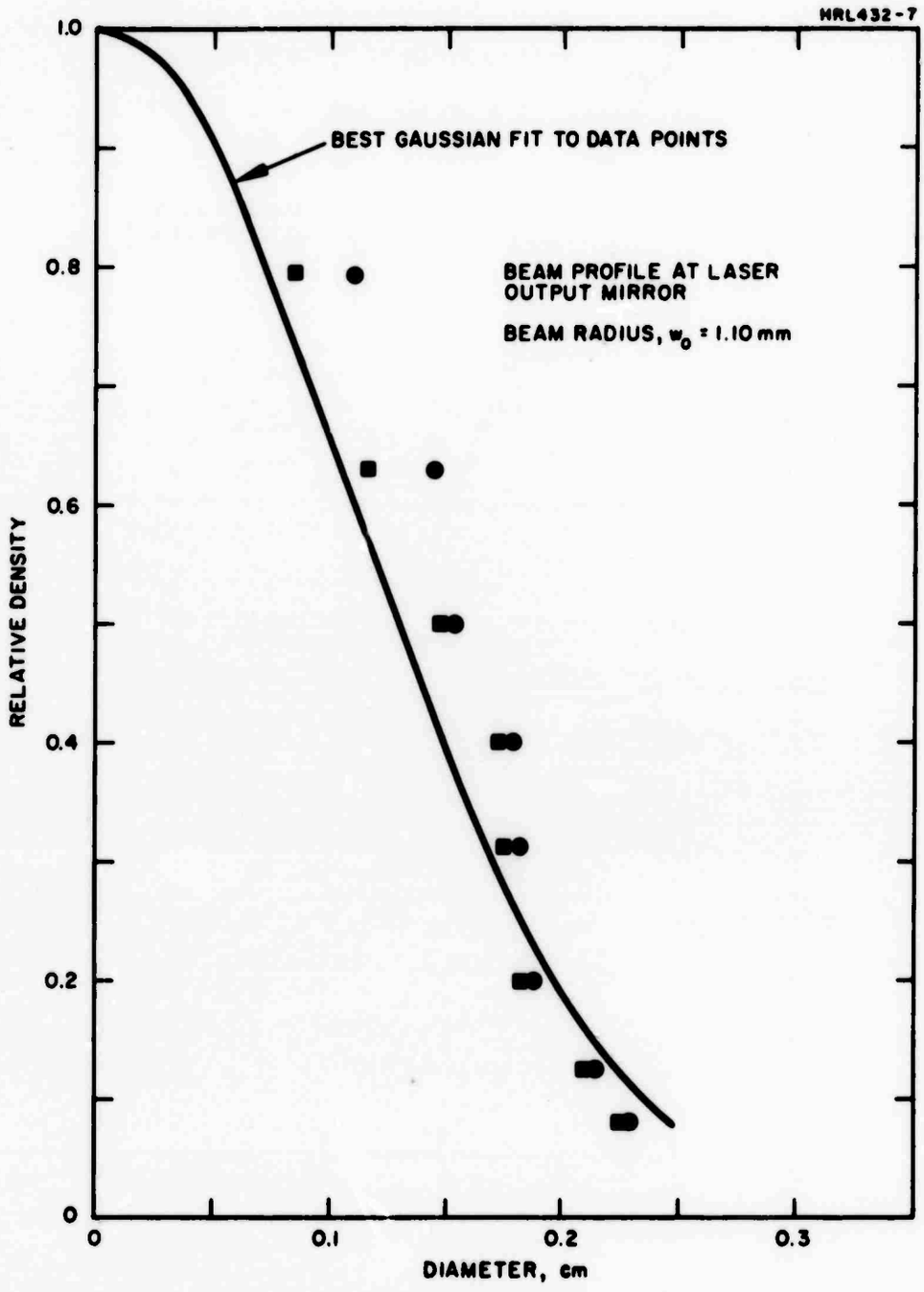

Fig. 5. Beam Profile Taken at Laser Output Mirror Compared with Computer Gaussian Fit.

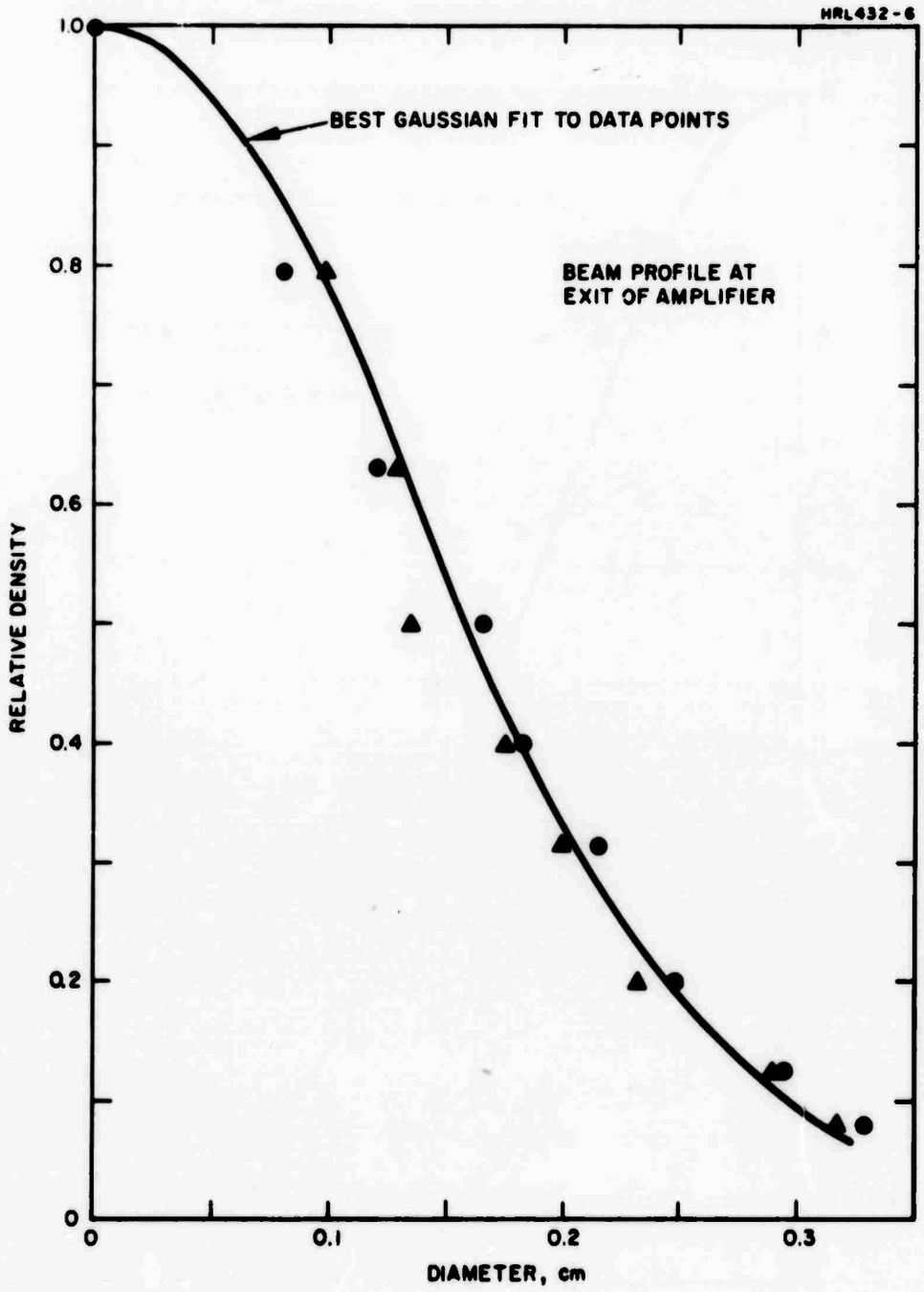

Fig. 6. Beam Profile Taken at Exit Plane of Amplifier Compared with Best Gaussian Fit.

traces. Since the scans are so noisy, the location of the peak is not easily defined. We see that, in general, the scatter is greater near the peak of the curves in Figs. 5 to 8 than in the wings, which is to be expected from the above consideration.

In making these measurements, at times we have also seen a varying deviation from radial symmetry of the photographed spots. This seems to occur much more often in the amplified beam, but we don't have enough measurements on the unamplified beam to be certain. We have found, however, that slight intentional misalignment of the amplifier does cause a marked deviation from radial symmetry of the photographed spot. As we point out later, since the lensing in the pumped amplifier is quite marked and probably very nonspherical, one might expect to obtain aberrations for off-axis propagation of the laser beam. However, the question as to why this elliptical spot sometimes appears for one shot, under apparently the same conditions as a previous shot where it was absent, is unknown. It may be that slight drifting of the oscillator alignment results in occasional off-axis propagation in the amplifier. If this is true, the drifting is too small to be detected with our alignment setup.

The main purpose of the densitometer scan data was to determine how closely the beam profile can be approximated by a gaussian distribution. We see that in most cases the agreement is fairly good, but as we will discuss later, we cannot accurately predict the behavior of the beam with respect to spot size, divergence, etc. solely by use of the propagation equations. Nevertheless, the approximation to a gaussian is a good one. Bearing this in mind, we continued our spot size measurements using Polaroid film instead of the spectroscopic plates. We chose to do this because of the great time involved both in processing the plates and in scanning them with the microdensitometer. When we use high contrast film (Polaroid Type 410 or IR film) we observe a series of spots of varying diameter on the film. Assuming a gaussian distribution we can determine the characteristic width from a knowledge of the diameters and relative exposures of the spots. This information for only two spots would be sufficient to determine the characteristic width but the use of all nine enables us to obtain a more reliable figure. An example of one of these photographs is shown

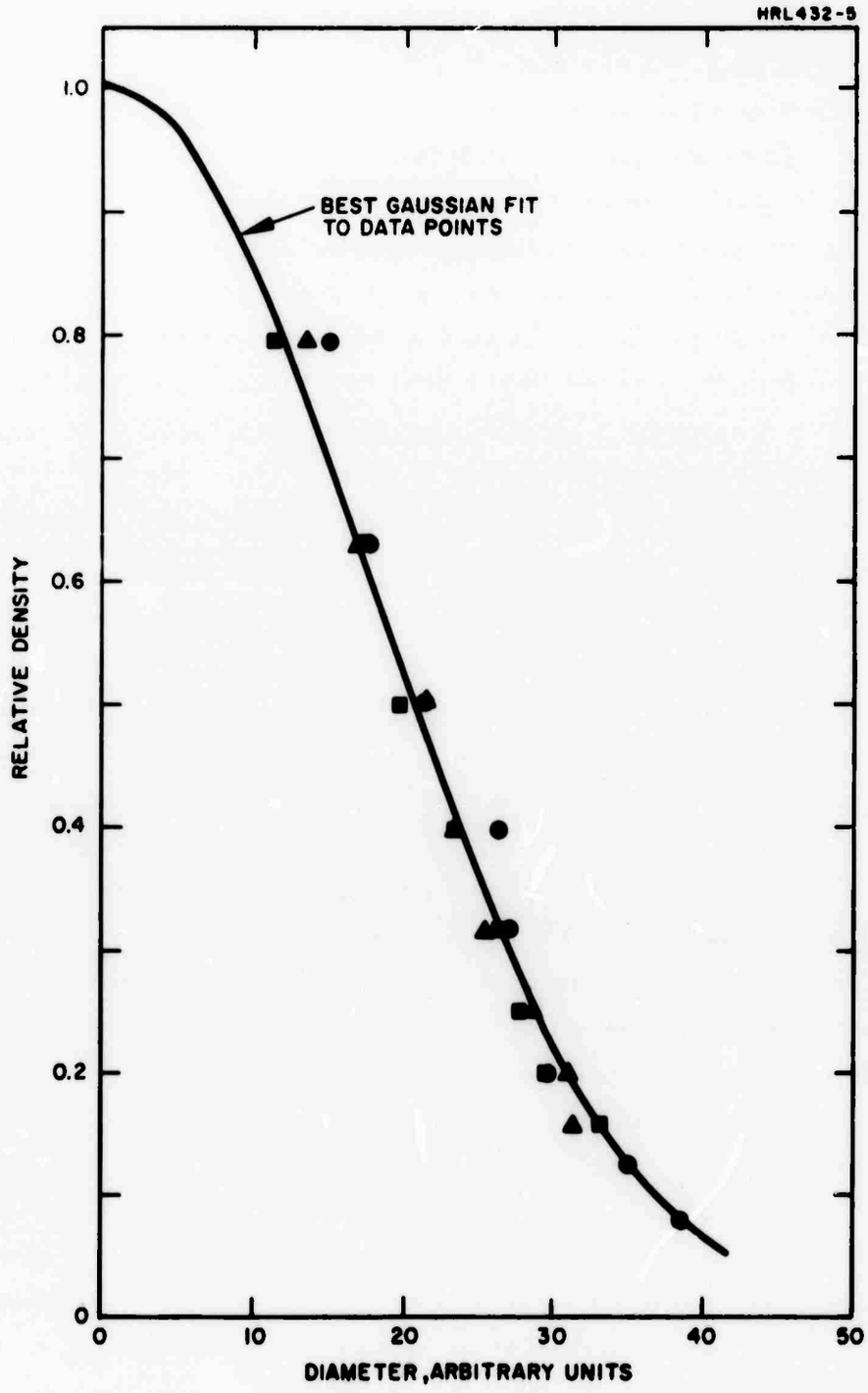

Fig. 7. Far Field Beam Profile for Unamplified Oscillator Taken in Focal Plane of 48.3 cm Lens Compared with Best Gaussian Fit.

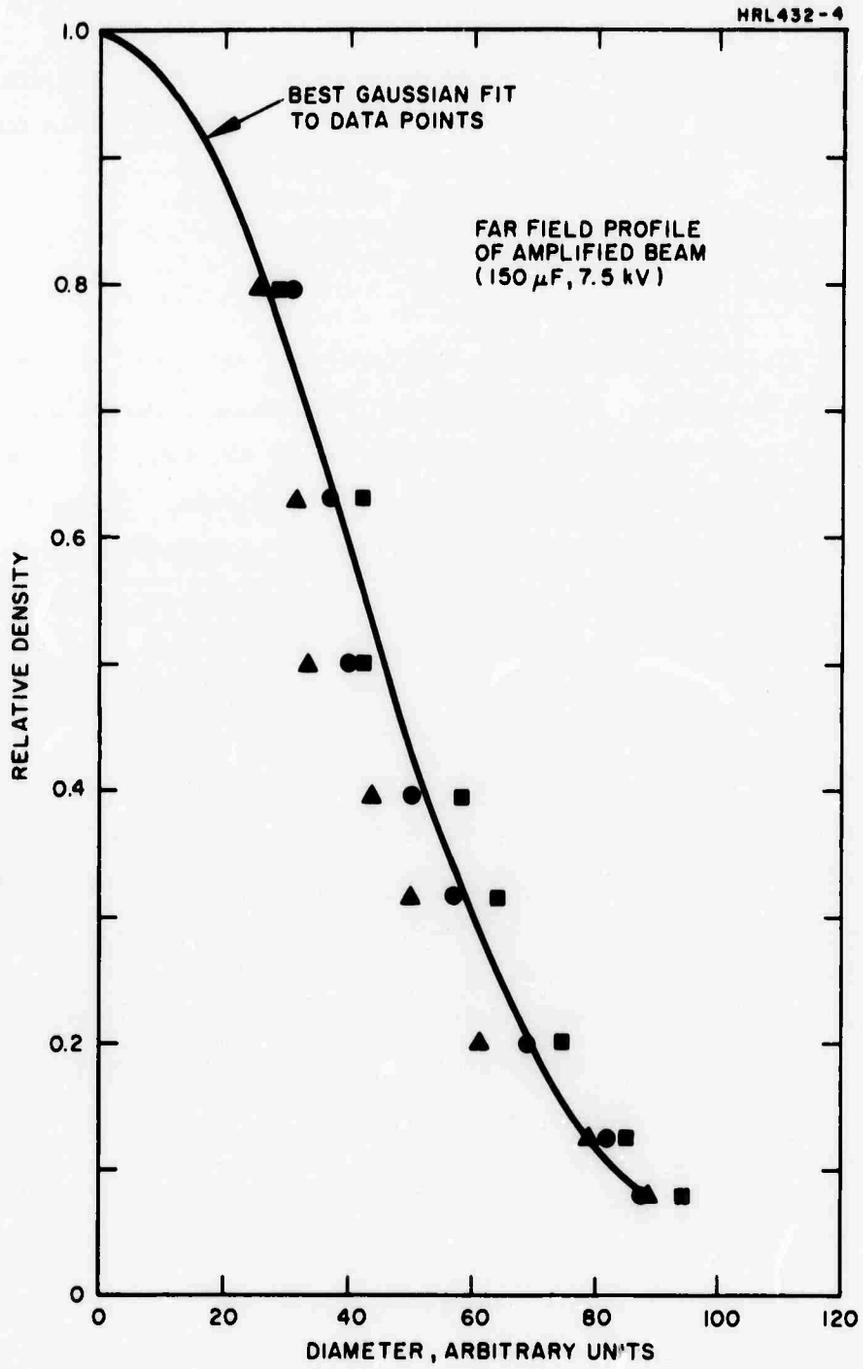

Fig. 8. Far Field Profile of Amplified Beam Taken in Focal Plane of 48.3 cm Lens Compared with Best Gaussian Fit.

in Fig. 9. The computer program used for the densitometer scan data was modified to handle the new situation and the data was more quickly processed.

C. DIVERGENCE MEASUREMENTS

We have measured the far field divergence of the laser beam both with and without amplification. This was accomplished by measuring the spot size in the focal plane of the 48.3 cm lens used in most of our previous damage threshold measurements. A few measurements were also made with an f = 19 cm lens. The results of densitometer scans from these measurements are shown in Figs. 7 and 8. The far field divergence of the oscillator alone is 0.35 mrad (half-angle). This value is the average of three separate measurements which agree to about 5 percent. The divergence of the laser after passing through the amplifier depends upon the extent to which the amplifier is pumped. The results of a number of measurements taken for different amounts of amplifier pumping are shown in Fig. 10. The measurements were taken in the focal plane of both the 48.3 cm and 19 cm lens. In the former case, the data came from densitometer scans of I-N plates; in the latter case, the data came from measurements of spots on Polaroid 410 film and Polaroid IR film assuming a gaussian distribution.

From these more accurate measurements of beam divergence we see that there is a substantial disagreement between the calculated divergence (0.20 mrad based on the measured radius at the output of 1.1 mm, $\theta = \lambda/\pi w_o$) and that observed for the unamplified oscillator (0.35 mrad). This apparently arises from the appreciable truncation observed in the beam profile at the oscillator output plane. This leads us to conclude that we cannot use the mode propagation equations to compute spot size, and hence energy densities of the focused beam using the spot size at the laser output mirror as an initial condition.

M 7686

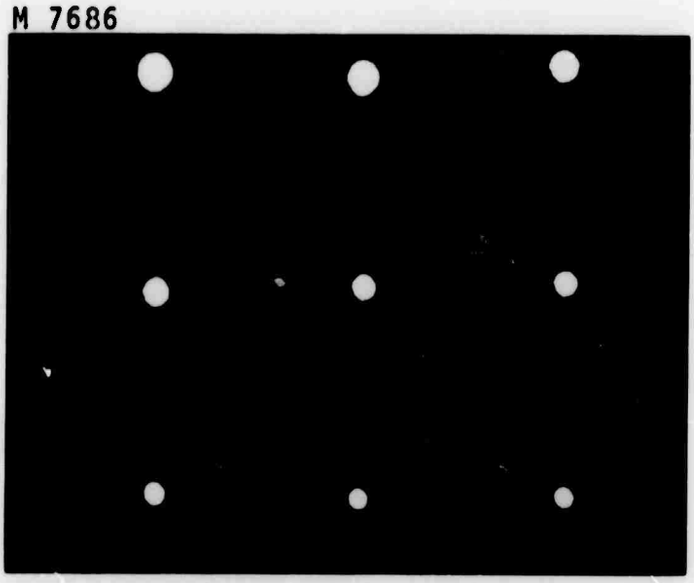

Fig. 9. Polaroid Photograph of Multiply Exposed Laser Beam Profile.

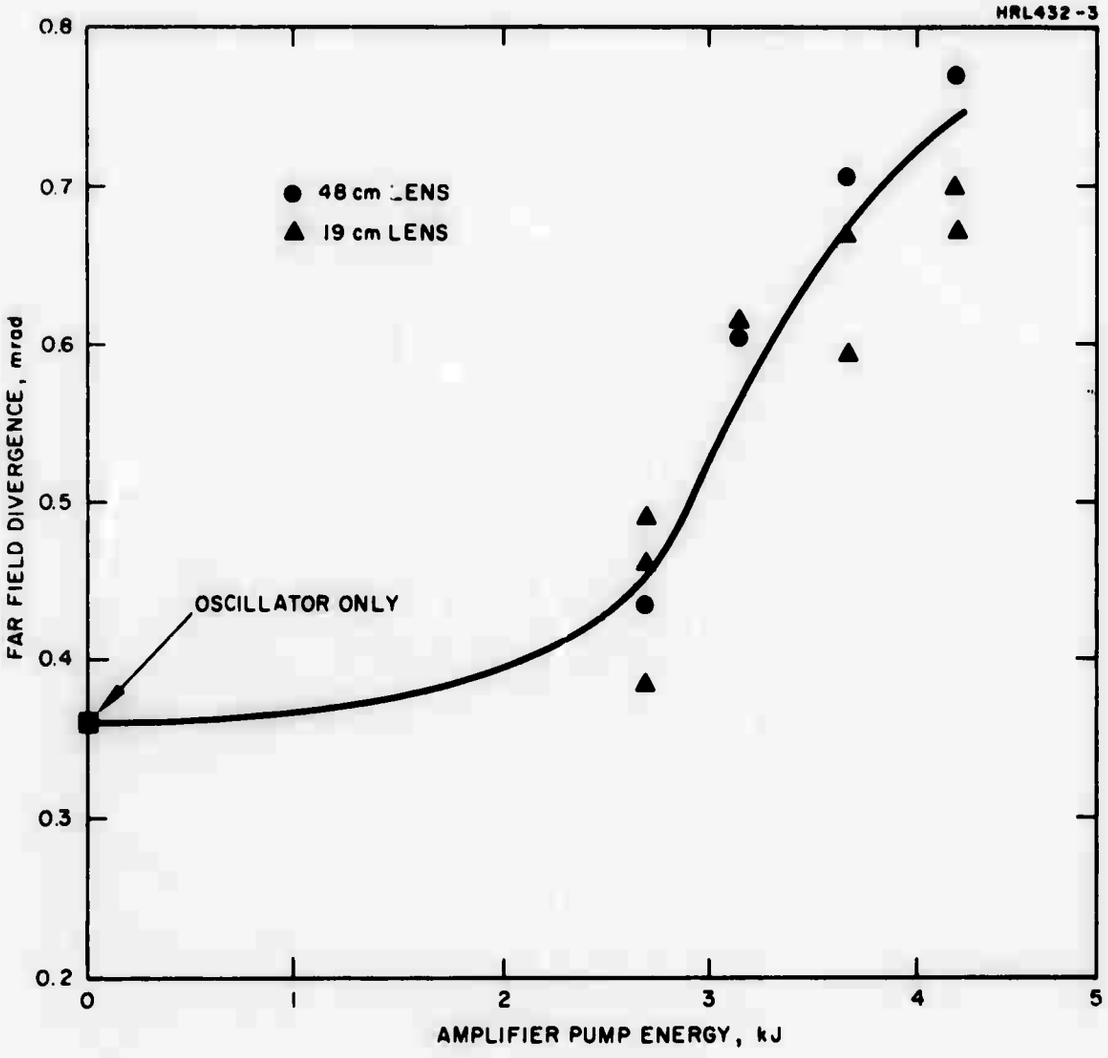

Fig. 10. Far Field Divergence of Laser Beam Versus Amplifier Pump Energy Measured in Focal Planes of 48.3 cm and 19 cm Lenses.

D. MEASUREMENT OF SIZE AND LOCATION OF BEAM WAIST

We have measured the size of the beam by the above described techniques for different points after the focusing lenses that were used to determine the previously reported damage thresholds. At this time we have made the measurements for the 48. 3 cm and 19 cm lenses only. The results for the 48. 3 cm lens were obtained from densitometer scans of Kodak I-N plates, while those for the 19 cm lens were obtained from spot size measurements on Polaroid 410 film and Polaroid IR film. These are shown in Figs. 11 and 12. We see that the minima are somewhat shifted downstream from the focal plane because of the negative lensing of the amplifier. The degree of this shift depends on the pumping. This is illustrated in Fig. 12, which shows the location of the minimum for two different pumping conditions representing essentially the extreme conditions of amplifier pumping in our previous threshold experiments. Since the lens is in the far field of the focused spot, the radius of the curvature of the phase fronts to the right of the lens is essentially equal to the distance from the lens to the minimum (with opposite sign). If the radius of the curvature of the phase fronts incident on the lens r_{in} is very large compared to the focal length, then the radius of curvature to the right of the lens r_{out} equals the focal length

$$r_{out} = \frac{f r_{in}}{f - r_{in}} \quad , \tag{1}$$

For $r_{in} \gg f$, $r_{out} = -f$ and the minimum occurs in the focal plane.* In our case the lens focal length is not negligible compared to the input radius of curvature; hence the output radius of curvature is somewhat larger than the focal length.

*The exact expressions are $s_{min} = - r_{out}/1 + \rho^2$ and $w_{min} = - r_{out} \lambda/\pi w_{lens}/(1 + \rho^2)^{1/2}$ for the distance from the lens to the minimum, s_{min} and the minimum spot size, w_{min}, where $\rho = r_{out} \lambda/\pi w_{lens}^2$. But for all our conditions $\rho^2 << 1$ and the equations simplify to those given in the text.

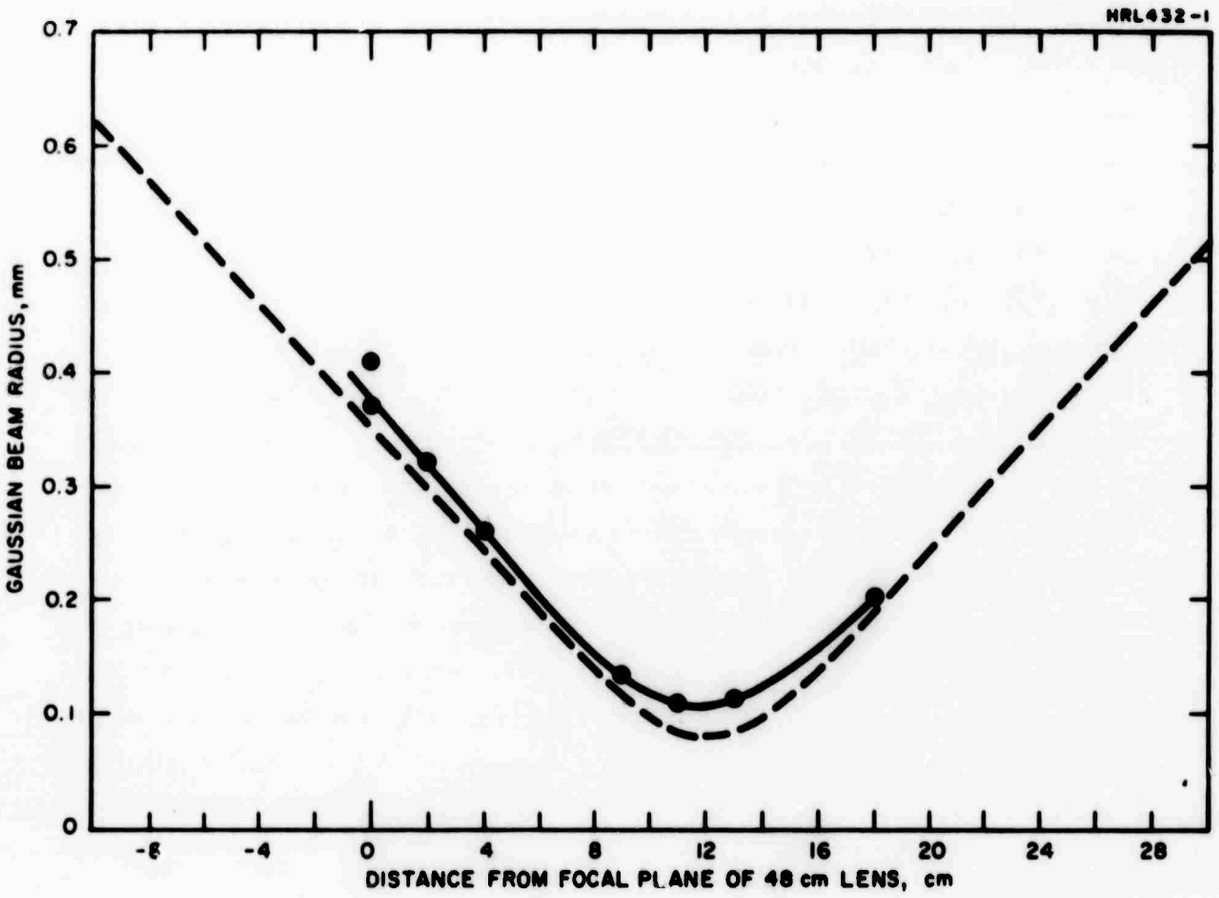

Fig. 11. Gaussian Beam Radius Versus Distance From Focal Plane of 48 cm Lens. The Dashed Curve is Calculated on the Basis of the Measured Spot Size at the Lens and Measured Beam Divergence. (Amplifier pumping — 150 μF, 7.5 kV).

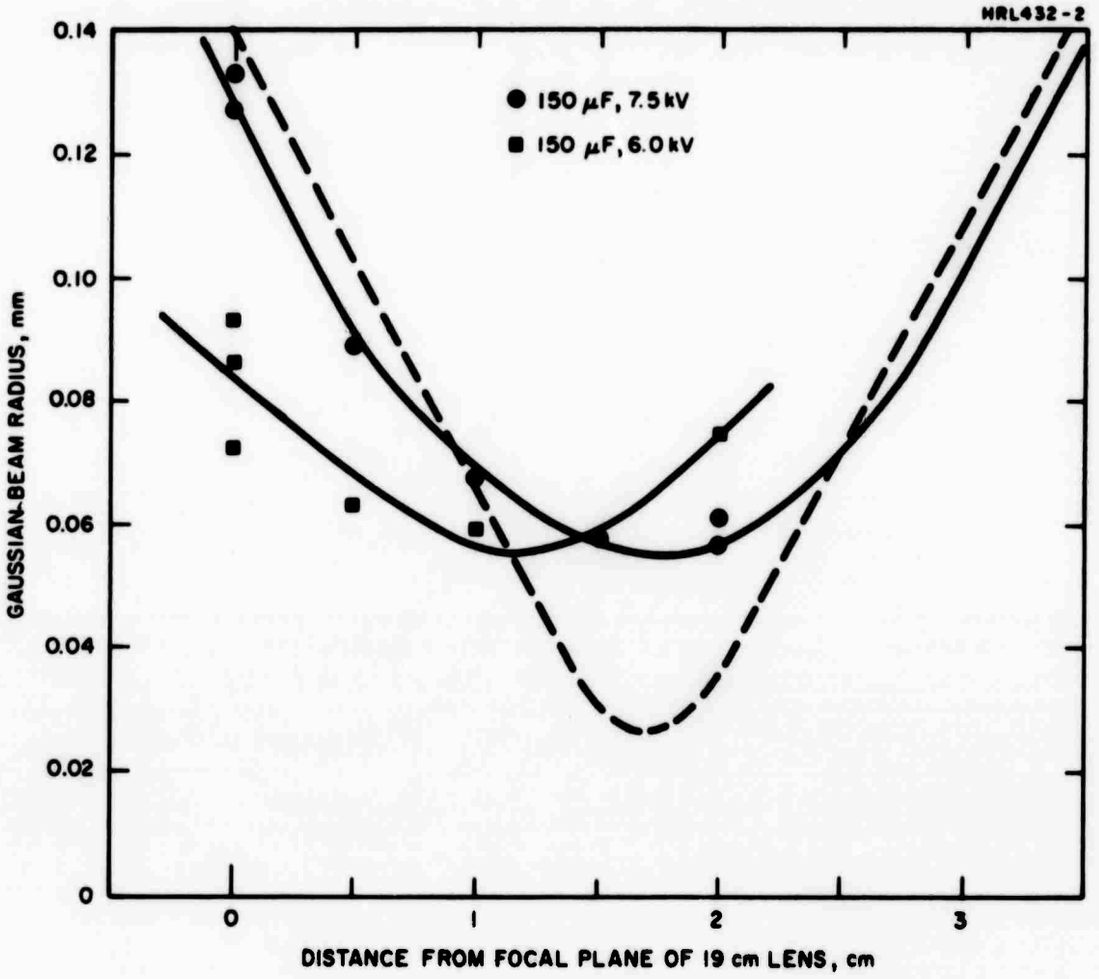

Fig. 12. Gaussian Beam Radius Versus Distance from Focal Plane of 19 cm Lens for Two Different Conditions of Amplifier Pumping. The Dashed Curve is Calculated on the Basis of Measured Spot Size at Lens and Measured Beam Divergence for Pumping Conditions — 150 μF, 7.5 kV.

If we take as our starting conditions $r_{out} = -60$ cm from the measured location of the minimum for the 48.3 cm lens, then we can compute the incident radius of curvature from

$$r_{in} = \frac{f r_{out}}{f + r_{out}} \quad . \tag{2}$$

We obtain $r_{in} = 240$ cm.

Using this value of r_{in} we can compute the radii of curvature and hence the position of the minimum for the other lenses. This is summarized in Table I.

TABLE I

POSITION OF BEAM WAIST FOR DIFFERENT FOCAL LENGTH LENSES

Radius of Curvature of Phase Fronts Incident on Lens = 240 cm (Amplifier Pump – 150 μF, 7.5 kV)			
Lens Focal Length (cm)	Radius of Curvature after Lens r_{out} (cm)	Distance of Beam Waist From Lens (cm)	
		(Present)	(Previous)[a]
48.3	-60	60	49.8
30.4	-34.6	34.6	31.1
19.0	-20.7	20.7	19.2
12.1	-12.7	12.7	12.2
8.5	- 8.8	8.8	8.5

[a]Calculated from assumptions listed in Section B.

A comparison of the measured spot size at the beam waist (Figs. 11 and 12) for the two lenses indicates an inconsistency. It is easy to show that the minimum spot size for a given lens is proportional to the radius of curvature of the phase fronts leaving the lens, r_{out}, under given input conditions

$$w_{min} = \frac{-r_{out}\lambda}{\pi w_{lens}} \quad . \qquad (3)$$

*

Therefore, we expect that the ratio of spot sizes for the 48 cm lens to the 19 cm lens should be 60/20.7 = 2.9, but we see that the measured spot size ratio is about 0.1/0.055 = 1.8, a fairly large discrepancy.

From (3) we can compute the spot size at the beam waist for the two different lenses and compare this with the measured values. Taking the values of r_{out} from Table I and the measured spot size at the lens, w_{lens} = 0.17 cm (amplifier pump 150 μF, 7.5 kV) we compute the values as shown in Table II.

The apparently fair agreement between the two measured results and the early calculated results in Table II is fortuitous. The early calculated results assumed that the amplifier does not affect the beam divergence, which we know is a false assumption. Also we see from Table I that the location of the minimum based on the same early calculated results is very much different from that actually observed.

---

*The exact expressions are $s_{min} = -r_{out}/1 + \rho^2$ and $w_{min} = -r_{out}\lambda/\pi w_{lens}/(1+\rho^2)^{1/2}$ for the distance from the lens to the minimum, s_{min} and the minimum spot size, w_{min}, where $\rho = r_{out}\lambda/\pi w_{lens}^2$. But for all our conditions $\rho^2 << 1$ and the equations simplify to those given in the text.

TABLE II

MEASURED AND CALCULATED BEAM RADII FOR DIFFERENT LENSES

Lens Focal Length (cm)	Beam Radius at Minimum (μm)		
	Early Calculated[a]	Revised Calculated[b]	Measured
48.3	104	78	100
30.4	65.2	45	–
19.0	40.2	27	55
12.1	25.6	16.5	–
8.5	17.8	11.4	–

[a] From propagation of 1 mm Gaussian assuming no effect of amplifier.

[b] From measured spot size at lens (1.7 mm) and measured divergence. (Amplifier pumping 150 μF, 7.5 kV.)

At this point it is not possible to be certain that the disagreement between calculated and measured spot sizes for the two different lenses (48 and 19 cm) is real or whether there is a limitation in the measurement. Since we have not yet measured the minimum spot sizes for the other lenses, we have no basis for further comparison at this time. It may be that the measured spot size for the 19 cm lens is limited by aberrations in the imaging system and that the actual spot size is, in fact, less than that. The fact that the beam divergences measured with the two lenses agree fairly well under similar conditions of amplifier pumping suggests that there may be a limitation in our measurement of the spot size at the minimum. On the other hand, the spot size may be limited by aberrations in the focusing lens itself. As we mentioned in our previous reports, the focusing lenses used in the damage threshold measurements were obtained from Special Optics and

advertised to give a diffraction limited focused spot for a range of beam sizes incident on the lens. Our lens spot size (1.7 mm) is well within the range specified for diffraction limited performance.*

A more reasonable idea as to the nature of the discrepancy will be possible when the spot sizes for the other lenses are measured and when the degree of reproducibility of the measurements is more reliably established. But as we shall see in Section H, the whole question as to the spot size as approached so far may be really an academic one, at least as far as the measurements in ruby are concerned.

E. AMPLIFIER LENSING

Since the divergence of the laser is increased on passing through the amplifier, and since the location of the focused spot is shifted downstream from the focal plane, we conclude that the amplifier acts as a negative lens. We can obtain a rough estimate of the effective focal length of the amplifier as a negative lens by the following considerations. From the location of the focused spot we obtain a radius of curvature of the phase fronts leaving the focusing lens, and from Eq. 1 we compute the incident radius of curvature. For the amplified beam and the 48.3 cm focal length lens we have $r_{out} = -60$ cm, and hence $r_{in} = 240$ cm. For the unamplified beam the location of the focused spot has been measured approximately using the 30.5 cm lens. In this case the minimum is found to be about 31.5 cm from the lens. This value of $r_{out} = -31.5$ cm gives $r_{in} = 960$ cm. The value for r_{in} calculated from the mode propagation equations is 2180 cm assuming a gaussian beam with the measured initial radius of 0.11 cm propagating a distance of 1.5 m

*The manufacturer claims essentially diffraction limited performance for f-values of 6 or greater with these specially designed lenses. In our case for the 19 cm lens, the f-value is 50 or greater, easily satisfying this requirement. The f-values in the imaging system which uses the same quality lenses are even larger.

from the laser to the lens. By comparing the measured and calculated far-field divergence, we found that the propagation equations do not accurately describe the behavior of the beam.

If we calculate the initial gaussian beam radius which would yield a radius of curvature of 960 cm after having propagated 150 cm from the waist, we obtain a value of 0.089 cm, a value about 20% less than the measured value. We will use this effective initial value for the beam radius of curvature for the unamplified beam at the exit plane of the amplifier which is located 60 cm from the focusing lens (90 cm from the laser). To calculate the radius of curvature at the amplifier exit plane for the amplified beam we use, as initial conditions, the known spot size (0.17 cm) and radius of curvature (240 cm) at the focusing lens and the lens-amplifier distance of 60 cm. The results of these computations for the radii of curvature of the phase fronts at the amplifier exit are: for unamplified beam, r = 1530 cm; for amplified beam, r = 182 cm. Thus, the amplifier can be thought of as a lens which changes the radius of curvature of the phase fronts from 1530 cm to 182 cm. The focal length of this lens can be evaluated from the expression $f = - r_{in} r_{out} / (r_{in} - r_{out})$ where r_{in} and r_{out} are the radii of curvature without and with amplification, respectively. We compute an effective focal length for the amplifier of - 207 cm. This value pertains to the conditions of maximum amplifier pumping studied (150 μF, 7.5 kV). Thus we conclude that the amplifier acts as a relatively mild, but nevertheless a significant negative lens.

F. SUMMARY OF BEAM PROFILE MEASUREMENTS

At this point let us examine the original assumptions listed in the first part of Section B, and comment on their validity based on the measurements we have made to date. First we have seen that there is a substantial deviation from gaussian behavior at the laser output mirror and that the measured beam divergence disagrees with that calculated for the

closest gaussian fit by a factor of about 1.5 We also note that we find beam profiles much closer to gaussians when we look in other regions, e.g., the far field. In addition, we find that the beam is defocused on passing through the amplifier to the extent that the divergence doubles for the most extreme pumping conditions. This results in a downstream shift in the location of the focused beam waist. The relative extent of this shift depends on the focal length of the lens giving the largest relative shift for the longest focal length. Thus in the case of the 48.3 cm lens used in many of the early damage threshold experiments, the beam waist is found to be beyond the exit surface of the samples studied. This is also true for the 30.4 cm lens used in some of the later experiments. For the other lenses, the beam waist occurs inside the sample, but not in the center as expected from the initial assumptions made in the early stages of this study. Incomplete results on minimum spot size measurements show a disagreement between measured values and those calculated on the basis of measured divergence and beam size at the lens. Further measurements are needed to determine the nature of this discrepancy.

G. REEVALUATION OF PREVIOUSLY REPORTED THRESHOLD DATA

On the basis of these observations we are in a position to reevaluate the threshold data presented in the previous report. Because of the fact that the actual minimum spot occurs outside the sample for the 48 cm lens, our actual power densities are somewhat lower than the previously reported values. Essentially in the case of the 48 cm lens, our samples have been subjected to a converging beam with the highest power density occurring at the sample exit surface. For the 19 cm lens, the measured spot is somewhat larger than the spot calculated from the early considerations, and therefore the damage thresholds measured with this lens are also revised downward. Based on these revised spot sizes and a more recent calibration of our TRG thermopiles, we present in Table III a revised set of damage thresholds for samples previously studied.

TABLE III

COMPARISON OF PREVIOUS AND REVISED
DAMAGE THRESHOLD VALUES

Sample	Previous Threshold (GW/cm^2)	Revised Threshold (GW/cm^2)
C_z Sapphire, L122 (19 cm lens)	12-17	8-11
Verneuil Sapphire, M118 (19 cm lens)	12	8
C_z Ruby, L105 (19 cm lens)	10-13	7-9
C_z Ruby, L105 (48 cm lens)	6-10	1.2-2
C_z Ruby, A100 (48 cm lens)	5-6	1-1.2
C_z Ruby, C124 (48 cm lens)	4-6	0.8-1.2
C_z Ruby, L104 (48 cm lens)	6-7	1.2-1.4
Verneuil Ruby, M119 (48 cm lens)	5-9	1-1.8

All power densities are given as gaussian spatial averages, $P/\pi w^2$ where P is the peak temporal power (Energy/Pulsewidth) and w is the gaussian beam radius (1/e point for $\vec{E}$).

T132

Let us emphasize here that the values reported for ruby in Table III are based on the assumption that the beam profile is smooth and approximately gaussian. We know from the forthcoming discussion in Section H that this is far from true. Nevertheless, we present the data based on the spot size measurements obtained in air.

H. SPOT SIZE MEASUREMENTS INSIDE SAMPLES

In this section we discuss the results of a few preliminary experiments where we measured the spot size inside both ruby and sapphire samples by the same techniques as that described in Section B. The obvious extension of the previous spot size measurements in air would be to continuously monitor from shot to shot the beam width inside a sample while performing the damage experiments. In this way we would have a direct measure of energy density rather than having to infer it from previous measurements. All the experiments described here were carried out using the 19 cm lens focused inside the particular sample. The pumping conditions in the amplifier were fixed at 150 μF and 7.5 kV, and the light intensity incident on the sample was varied by a pair of Glan-Kappa prisms, the first of which was rotated to the desired angle and the second of which was fixed so that the polarization was always the same inside the sample ($\vec{E}$ perpendicular to the C-axis).

The lenses and samples were placed so that the waist of the focused light beam, as determined by the measurements summarized in Table I would occur about 2 cm inside the exit surface of the sample. The plane being imaged in the photographs lies 0.5 cm upstream from the beam waist.

A number of photographs taken with the multiple-lens camera are shown in Figs. 13 and 14. The interesting result of this probing is that the beam profile begins to change radically in ruby at powers well below the damage threshold whereas for the sapphire the beam profile is essentially smooth all the way to and beyond the threshold for bulk damage.

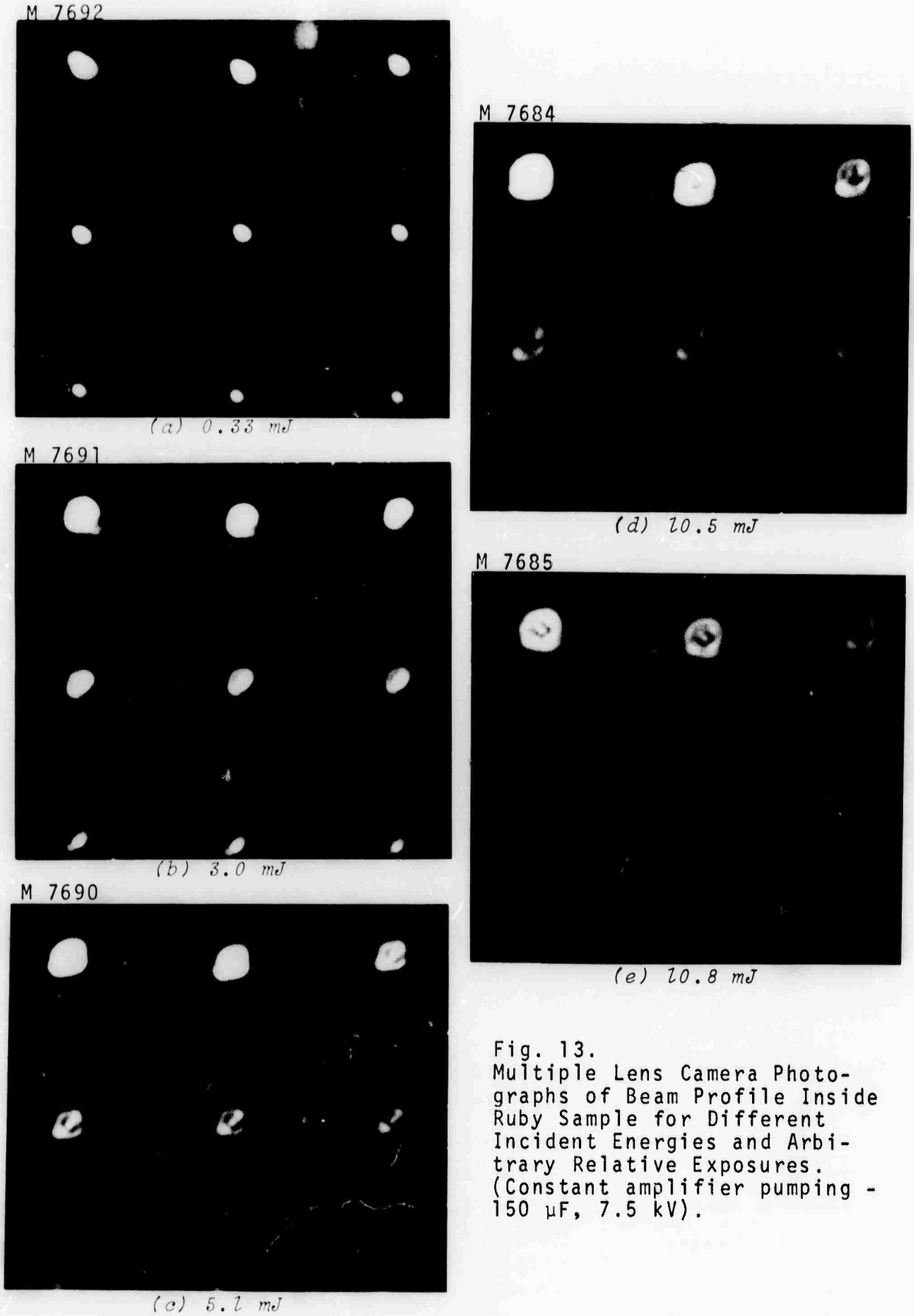

Fig. 13.
Multiple Lens Camera Photographs of Beam Profile Inside Ruby Sample for Different Incident Energies and Arbitrary Relative Exposures. (Constant amplifier pumping - 150 μF, 7.5 kV).

M 7688

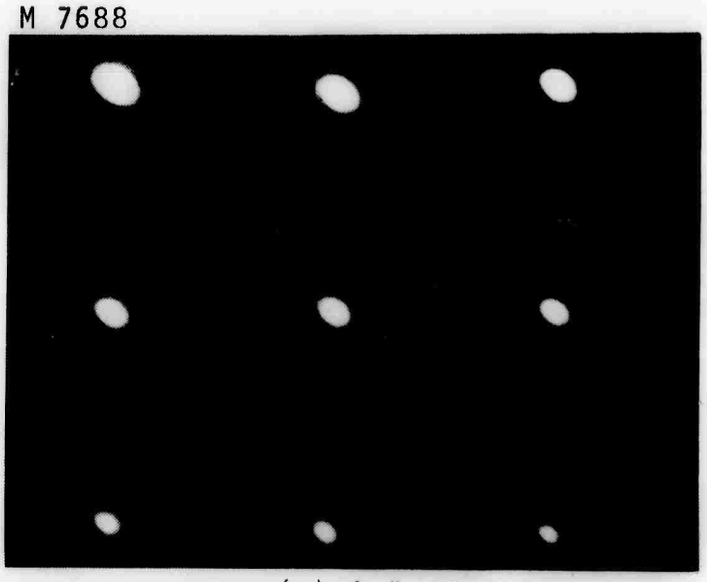

(a) 0.3 mJ

M 7687

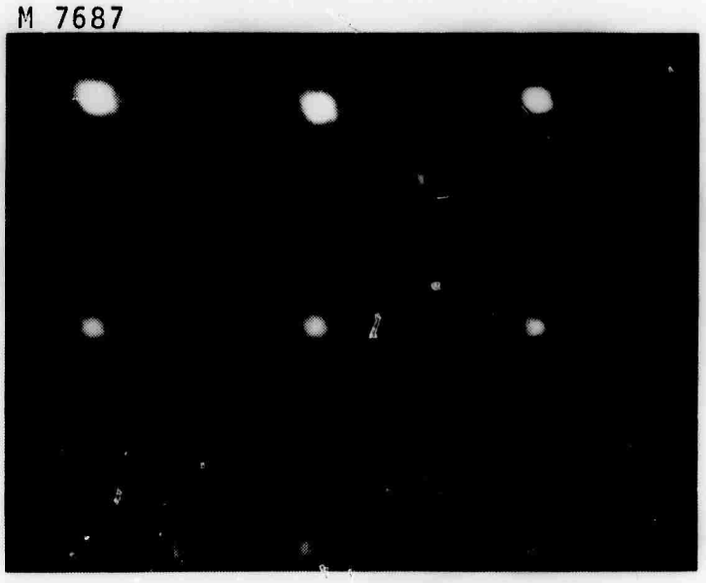

(b) 25 mJ

Fig. 14.
Multiple Lens Camera Photographs of Beam Profile Inside Sapphire Sample for Different Incident Energies and Arbitrary Relative Exposures.

We wish to emphasize here that all the photographs were taken in the same plane in the sample and that the only parameter that was varied was the amount of energy incident on the 19 cm focusing lens. We see from Fig. 13(a) that at low incident energy (0.33 mJ) the beam profile is smooth, but that by the time we reach 3 mJ (Fig. 13(b)) we begin to see what appears to be a bright central spot with a less bright peripheral halo. (In these experiments, the laser pulse width was about 30 nsec, FWHM.) At higher incident energies we see a variety of patterns in the beam profile. We note also that the threshold for internal damage in this particular sample measured under the same conditions is 30 mJ incident on the focusing lens and that the threshold for exit surface damage is about 10 mJ. Thus we see these effects of beam distortion well below the threshold for any catastrophic phenomena.*

The whole question of measurement of energy density inside ruby samples by measuring spot sizes assumes a completely different aspect in the light of these drastic changes in the beam profile. Obviously, it would be extremely difficult to determine energy densities in these peculiar spatial distributions. Thus the data presented in Sections G and I must be completely reevaluated in the light of this new information.

When we examine sapphire under the same conditions as those described for ruby, we see no such behavior. Fig. 14 shows photographs taken under two extreme conditions. Fig. 14(a) was taken at low incident energy (~0.3 mJ) and Fig. 14(b) at an energy higher than the bulk damage threshold, which was 20 mJ for this sample. For a large number of shots over this range of energies we saw no

---

*At present, we do not have sufficient data to locate the threshold for this beam distortion effect. We only know it lies between 0.3 and 3 mJ for the conditions described above.

irregularities in the beam profile. After reaching threshold for internal damage, we saw a general decrease in light reaching the imaging optics presumably because of side scattering from the damage sites.

Again we see an interesting difference in the behavior of ruby as compared with sapphire when subjected to intensive illumination at 6943 Å. It is reasonable to suspect that the beam distortion seen in ruby arises from thermal effects due to the absorption at 6943 Å. It would be interesting to make similar measurements on ruby while externally pumping. One might expect that at inversion this effect would disappear, if in fact it arises from absorption at 6943 Å.

I. RUBY DAMAGE THRESHOLD AS A FUNCTION OF LENS FOCAL LENGTH

Early in this reporting period we made a number of measurements of damage threshold in a given ruby sample as a function of focal length for a number of lenses ranging from f = 48 cm to f = 7.6 cm. The purpose of these measurements was to find a relationship between the damage threshold and the spot size of the beam inside the sample. The data were taken, and threshold power density was plotted versus beam radius using the assumptions that were outlined in the beginning of Section B. However, we have found that none of the assumptions is completely valid. Moreoever, even knowing the contribution which the amplifier makes to the beam divergence, it appears we cannot relate the focal spot sizes to each other in a simple way, i.e., that the ratio of the spot sizes equals the ratio of the focal distances. (The resolution of this question depends on further careful measurements of spot sizes for all the lenses and/or determination of the contribution of aberrations.) The uncertainty is further compounded by the more recent observation of the complex breaking up of the beam at relatively low powers in ruby, which makes the whole concept of spot size a very nebulous one.

Nevertheless, we will present the data in spite of the obvious uncertainty in the numbers. This is shown in Fig. 15. Data for the 48 cm and 19 cm lens are based on the more recently measured spot size data, even though there is some uncertainty concerning data on the 19 cm lens. The remaining data for the other lenses are based on the assumption of a diffraction limited spot at the minimum, the measured spot size at the lens, and measured divergence for the approximate pumping conditions.

We present these data to illustrate a trend which we believe is valid, even though the actual numbers are uncertain and may never be satisfactorily evaluated because of the beam distortion. We note that the slope of the plot in Fig. 16 is -1.8. From eq. (49) in the Appendix we see that a log-log plot of $P_{thr}/\pi d_o^2/4$ versus d_o would give a slope of -2 if the second term in the denominator were large compared to unity. The observed slope of -1.8 indicates fair agreement with this equation and may be taken as an approximate confirmation of a self-focusing mechanism.

J. STREAK CAMERA EXPERIMENTS

A series of experiments have been carried out to explore the time evolution of the damage tracks during formation. The setup is shown in Fig. 16. In early experiments we focused inside a Cz sapphire sample with the 19 cm lens. Based on subsequent spot size measurements described in Section E, we note that the beam waist occurs between 0.5 and 1 cm from the exit face of the sample. To time-resolve the damage we used an STL image converter camera operating in the streaking mode. The camera was set up to photograph the sample transverse

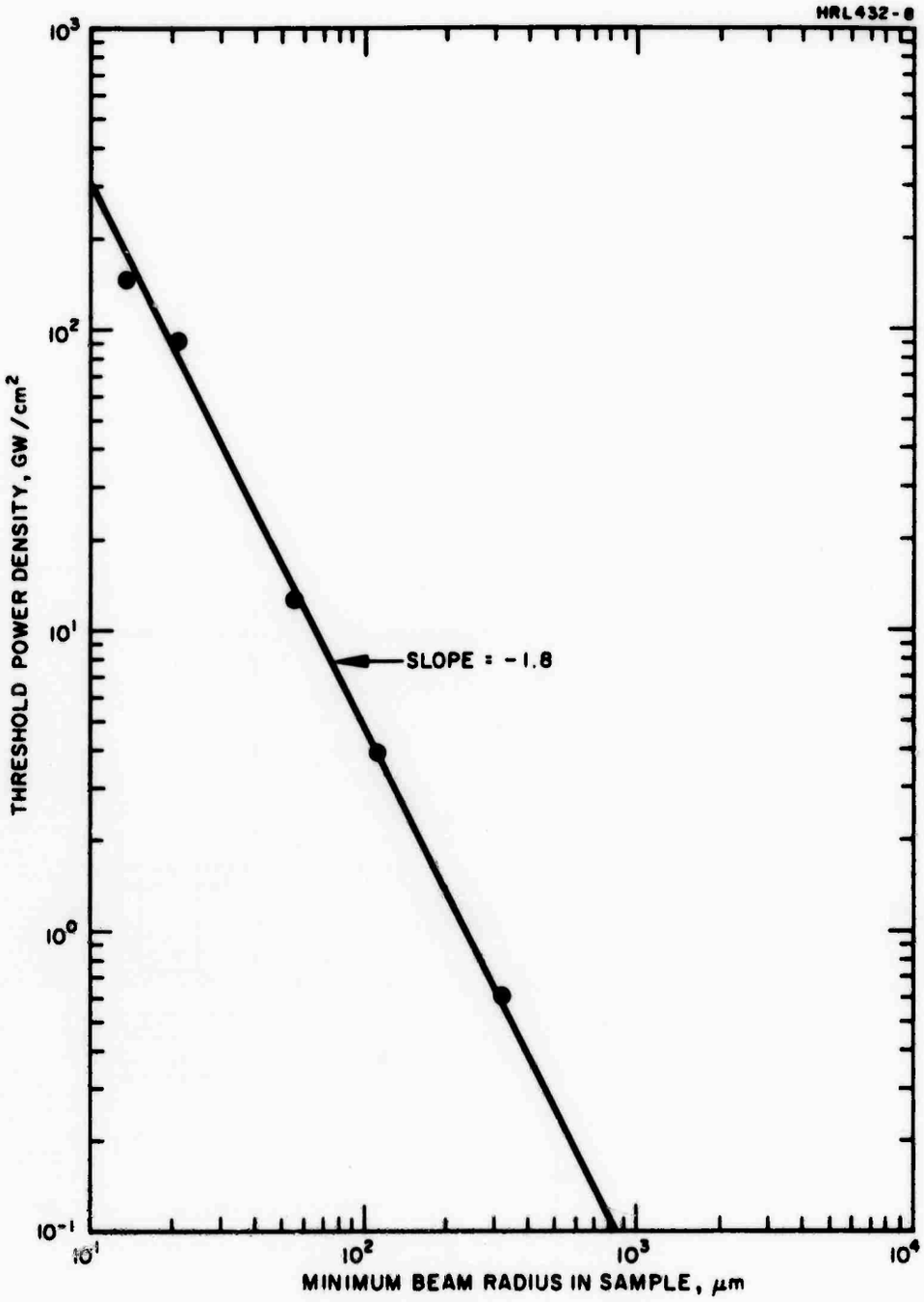

Fig. 15. Threshold Power Density Versus Minimum Beam Radius for Ruby Sample N 110.

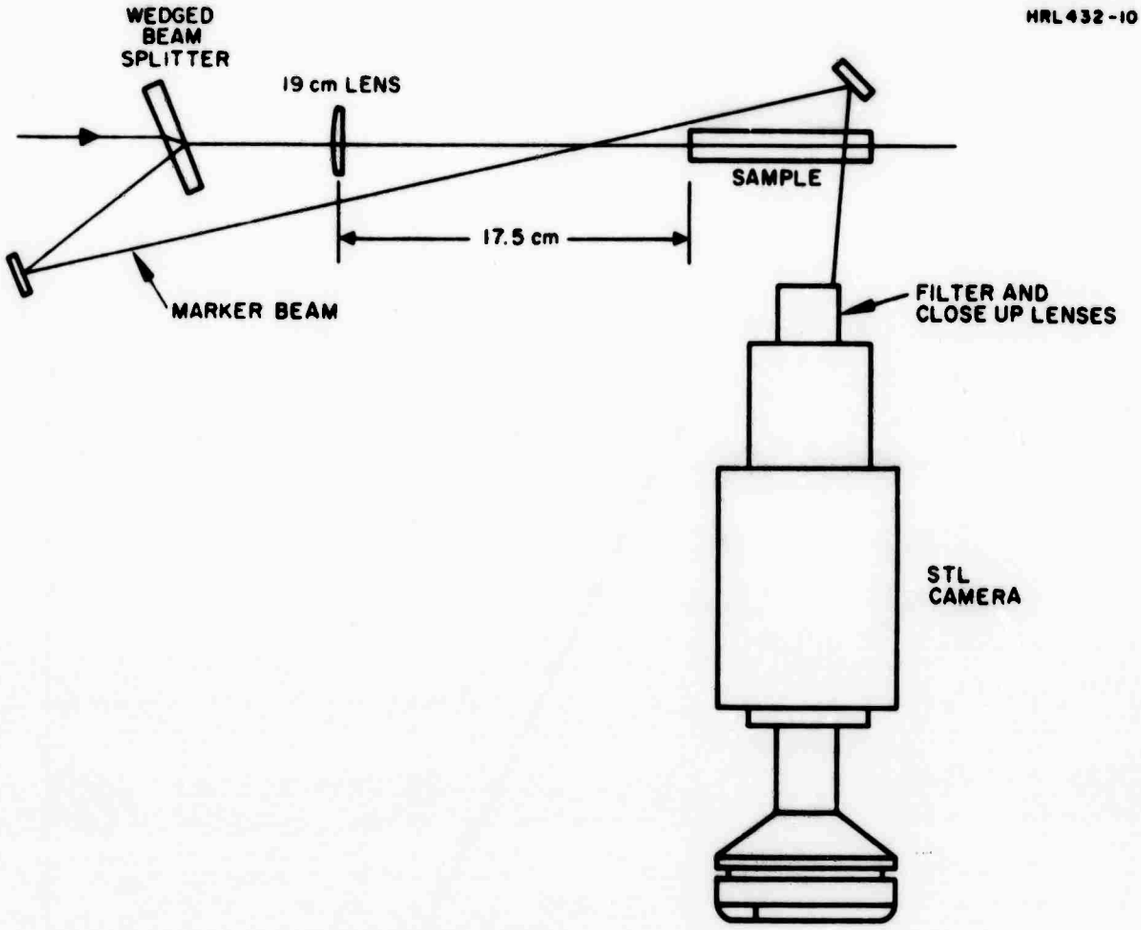

Fig. 16. Schematic Representation of Setup Used in Streak Camera Experiments.

to the direction of propagation of the laser beam. The laser was operated with a Pockels cell Q-switch instead of the cryptocyanine solution, so than an electronic trigger could be provided for camera shuttering. The laser pulse using the Pockels cell is from 30 to 35 nsec wide (FWHM) with a small amount of 750 MHz modulation. An oscilloscope trace of the laser pulse is shown in Fig. 17(a). A Corning 4-94 filter was used in front of the lens. This absorbs the side-scattered laser light while passing the light from the self-luminous tracks.* Typical streak camera photographs are shown in Figs. 18(a) and (b).

More recently we have obtained some streak photographs when Q-switching the laser with the cryptocyanine solution. In this case the pulses incident on the sample are unmodulated, with widths ranging from 16 to 20 nsec, as shown in Fig. 17(b). The camera was triggered by the light from the leading edge of the laser pulse using the amplified signal from a fast silicon photodiode. In these experiments we split off some of the incident light and passed it through the sample into the camera (see Fig. 16) to give a marker streak whose purpose is to show the relative times of the damage formation and the incident illumination. The difference in path length of the main beam and the marker beam is such that the marker beam arrives at the sample about 1 nsec later than the main beam. These are shown by the streak photographs in Figs. 19 and 20.

We see that the damage sites furthest from the laser are the first to form, and that the damage track grows in the upstream direction. This phenomenon was observed during some preliminary

*We have also looked at scattered laser light from the damage sites by placing a Wratten No. 70 filter in front of the streaking camera lens. Here we see essentially the same thing as we do when looking in the blue-green, but there is a great deal of light scattered from other damage sites formed in previous shots in the sample, giving rise to a background which makes the photographs more difficult to interpret.

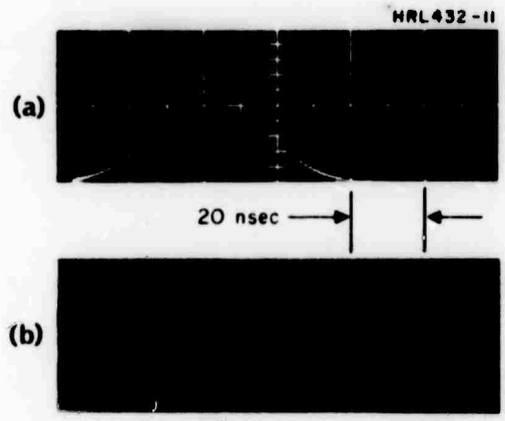

Fig. 17.
Oscilloscope Traces of Typical Laser Pulses Used in Streak Camera Experiments. (a) Modulated Pulse from Pockels Cell Q-Switch; (b) Unmodulated Pulse from Cryptocyanine Q-Switch.

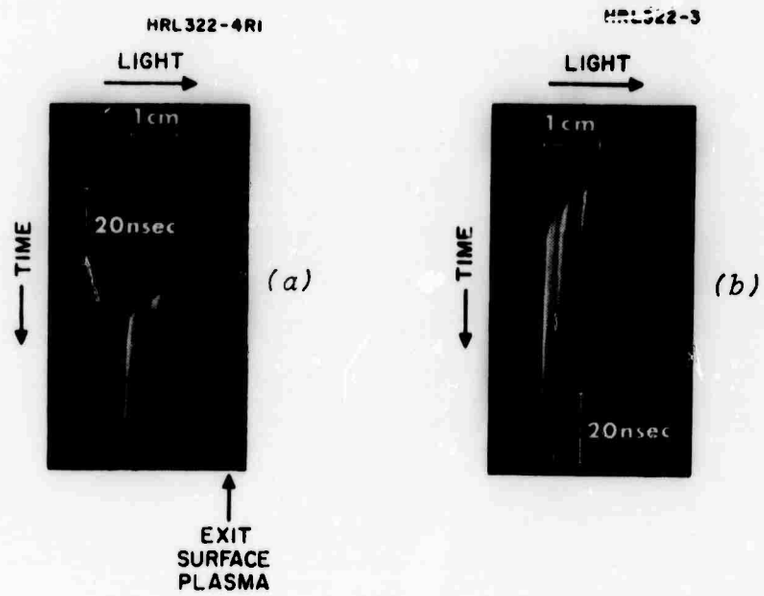

Fig. 18.
Streak Camera Photographs Showing Time Evolution of Damage Filaments in Sapphire. (Modulated laser pulse from Pockels cell Q-switch). (a) and (b) are at different magnifications.

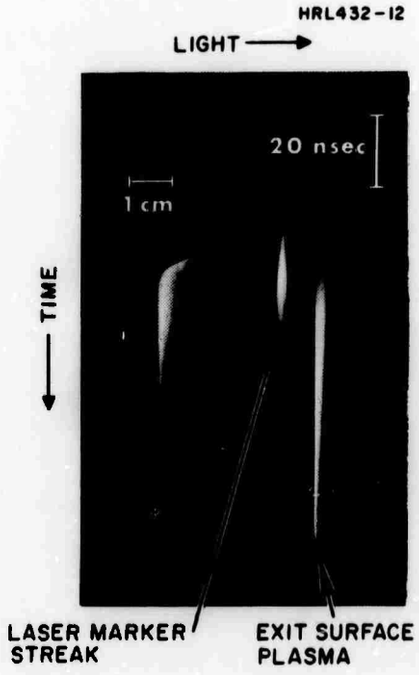

Fig. 19.
Streak Camera Photograph Showing Time Evolution of Damage Filaments in Sapphire. (Unmodulated pulse from cryptocyanine Q-switch).

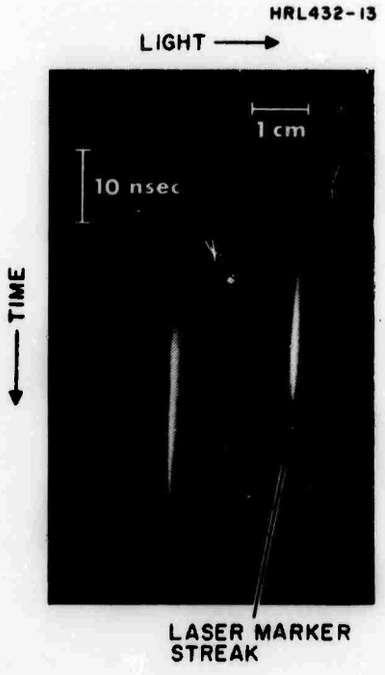

Fig. 20.
Streak Camera Photograph Showing Time Evolution of Damage Filaments in Ruby for Unmodulated Pulse. (Exit surface plasma is out of field of view).

experiments (unpublished) in glass at an early stage of HRL involvement in laser-induced damage (1964). By roughly measuring the slope of the streaks in the photographs we can compute an apparent rate of backward propagation of the damage. The results of some of these slope measurements are summarized in Table IV.

TABLE IV

APPARENT PROPAGATION VELOCITIES OF DAMAGE FILAMENTS

Sample	Propagation Velocity of Damage Track (cm/sec)	Laser Pulse Length (ns) (FWHM)
C_z Sapphire, L 123	$6.5\text{-}13.5 \times 10^7$ Ave-$10.0\text{-}10^7$ [a]	30-35 (750 MHz modulation)
C_z Sapphire, L 121	$13.7\text{-}41.5 \times 10^7$ Ave-25.3×10^7 [b]	16-20 (unmodulated)
C_z Ruby, L 108	$14.9\text{-}24.9 \times 10^7$ Ave-23.4×10^7 [c]	16-20 (unmodulated)

[a] Eight measurements

[b] Six measurements

[c] Seven measurements

T133

The backward moving damage track is consistent with the idea of a moving focus picture described qualitatively as follows. Since the characteristic self-focusing length is longer for low powers than for high powers, one would expect that light in the leading edge of the pulse would be self-trapped further downstream than the peak, hence a

self-trapped spot would be expected to move in an upstream direction. If this were the case, one might expect a different characteristic rate of propagation for incident pulses with different rise times.

By comparing the location of the most intense part of the laser marker streaks with the damage track locations, we can see (Figs. 19 and 20) that the damage track is formed before the incident laser light reaches its peak intensity. By comparison of the apparent propagation velocities in Table IV with the pulse widths, we see that the shorter pulses correspond to higher velocities as might be expected.

One possible explanation for the range in propagation velocities observed is that the streak rate in the camera may not be constant. It is possible that when the camera first turns on, it is not streaking as fast as it is after it reaches the latter stage of its sweep. Thus events which are observed in the early part of the camera sweep will appear to be separated by shorter times than those observed in the late part of the sweep. This is suggested by the appearance of the laser marker streak seen in Figs. 19 and 20. From the oscilloscope traces of these pulses (Fig. 17(b)), we see that the leading and trailing edges of the pulse are quite symmetrical; in the streak picture the leading edge seems to be longer than the trailing edge. It is not easy to see the intensity profile in the marker streaker because of the high film contrast, but the most exposed part of the streak seems to be definitely asymmetrically located with respect to the leading and trailing tails of the streak. Thus we suspect that the streaking rate is not constant. More detailed tests during the next report period will determine if this is in fact the case.

We also note two other features from these photographs. First, that the ruby damage track is shorter than the sapphire damage track for similar conditions of incident energy and focusing. Second, the modulated pulse gives a modulated track and the smooth pulse gives a smooth track, as seen by comparing Fig. 18 with Fig. 19 for sapphire. The frequency of the modulation on the streak camera photographs is the same as that on the corresponding laser pulse. This connection between the modulated pulse and the modulated track was also

suggested by some results presented in the last report. Recently, we were contacted by J. Marburger of the University of Southern California, who was made familiar with this work when the principal investigator gave a seminar at U.S.C. in October. He has been active in theoretical research on self-focusing phenomena and has indicated that these modulated streak photographs might give some measure of the nonlinear index of refraction for sapphire using his theoretical approach. The details of this possibility will be discussed later.

Within the next contract period, further streak camera measurements will be made with ruby and sapphire under conditions of different pulse length and focusing.

K. ADDITIONAL OPTICAL PUMPING EXPERIMENTS

In the last report we presented the results of a number of experiments where we optically pumped the sample while performing damage threshold measurements. We observed a large amount of scatter in the data because of interference from plasma formation at the entrance surface and were not able to state clearly whether or not the threshold is affected by optical pumping. In the early part of this reporting period we repeated the pumping experiments with better precision and found a slight decrease in threshold with optical pumping. This is shown in Fig. 21. The upper graph shows the recent more precise data for C_z Ruby, L107. The lower three graphs are data from the last report presented for comparison. We see about 20% decrease in relative threshold for the most extreme pumping case compared with the unpumped case.

We also discussed in the last report an interesting effect concerning the location of damage in the sample as a function of optical pumping of ruby. We noted that the beginning of the damage track (i.e., the upstream end) is shifted downstream with optical pumping.

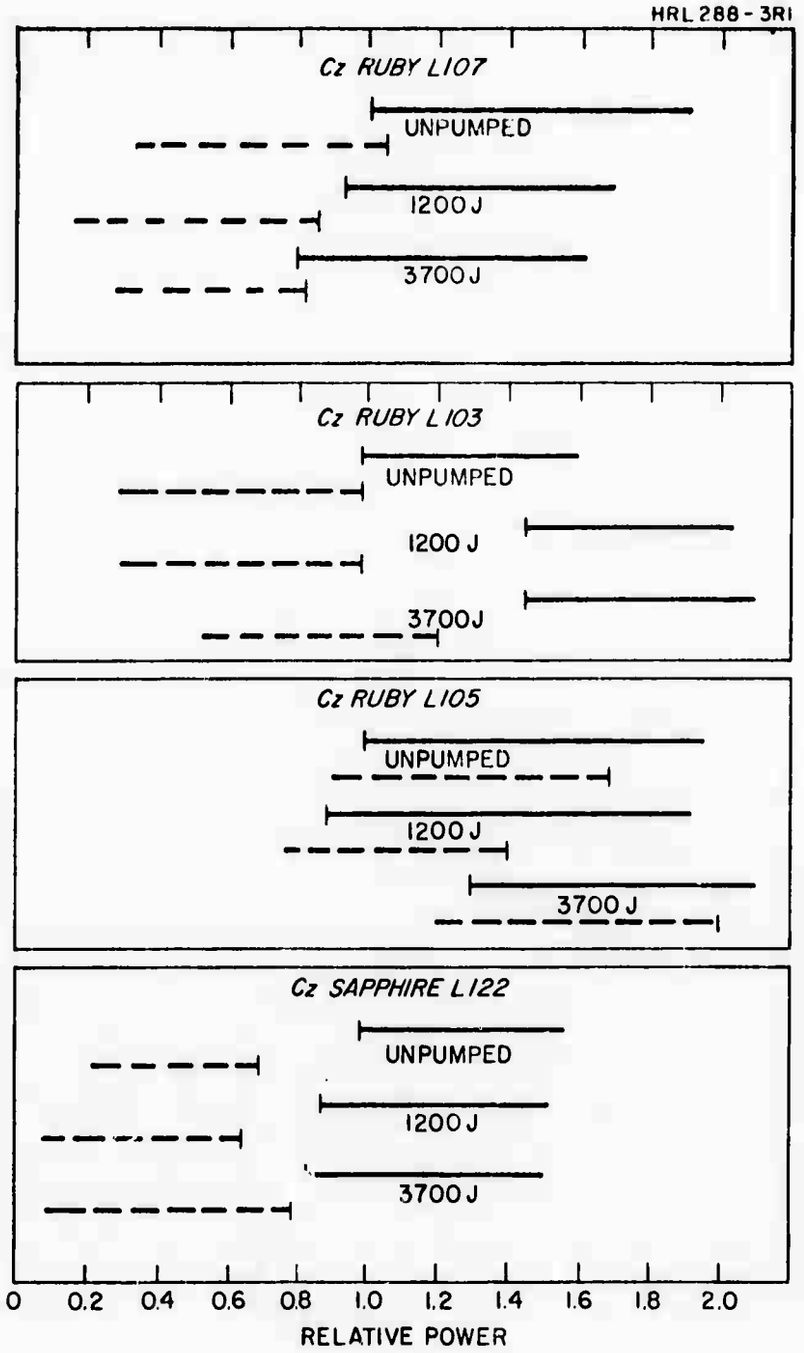

Fig. 21.
Relative Bulk Damage Threshold as a Function of Optical Pumping for Different Samples. The Thresholds are Normalized to Unity for the Unpumped Sample. Dashed Line — No Damage; Solid Line — Damage. The Three Lower Graphs are Reproduced from the Last Report; the Upper Graph Shows Results of More Reproducible Measurements Taken During this Reporting Period.

(We know now from the streak photographs that the upstream end of the damage track is really the last part which is formed.) From this shift in the damage track in ruby we inferred that the optical focus was shifting, but we now know from our beam profile measurements that the focus is located downstream from where we thought it was. In fact, from our more recent streak camera measurements we find that the damage track occurs upstream from the natural focus in the material. In sapphire, the track begins at or very close to the natural focus and progresses upstream; in ruby the points of beginning and end of the track occur substantially upstream from the natural (i.e., low power) focus. Optical pumping in ruby shifts the track toward downstream locations as well as making it longer. That is, it approaches the behavior for sapphire.

Details of this will be studied during the next period. Precise data on this point are not available at this time. However, we wish to point out that the shift in track location is not necessarily related to a defocusing due to pumping solely, but may be connected with the fact that pumped ruby behaves more like sapphire simply by virtue of its being pumped.

L. PRESENTATIONS MADE IN THIS PERIOD

During this reporting period, different aspects of this work were discussed in presentations at the ASTM Symposium on DAMAGE IN LASER MATERIALS at the National Bureau of Standards, Boulder, Colorado, June 24 and 25, 1970 and at the Sixth International Quantum Electronics Conference, Kyoto, Japan, September 7 to 10, 1970.

M. PLANS FOR NEXT PERIOD

During the next period we will complete the unfinished aspects of the work carried on in this period with emphasis on the beam profile measurements inside ruby. We will examine the beam profile at different locations in the samples to determine where and at what power the beam distortion first begins to appear. This will be done both with unpumped and pumped samples and with different focal length lenses. It will be interesting to see whether the behavior in the pumped samples approaches that of sapphire as the sample approaches inversion, as well as what happens when the sample exhibits gain. It will also be possible and perhaps informative to investigate the time evolution of the beam distortion with the STL camera. Now that we have characterized the beam properties under certain conditions we will determine carefully the location of the damage relative to the internal focus and attempt to correlate this with the results of Zverev and Pashkov[2] as well as to confirm some of their results regarding the length of the damage track as a function of incident power.

Additional streak camera studies will be carried out on the damage evolution in ruby and sapphire with an attempt to correlate the effective rate of propagation with pulse duration and laser power. Damage threshold versus lens focal length measurements will be obtained for sapphire and the results will be compared with the self-focusing theory.

BLANK PAGE

SECTION II

THEORETICAL STUDIES ON OPTICAL DAMAGE

A. INTRODUCTION

During the first half of the reporting period, the theoretical studies were carried out at a reduced level due to the involvement of the main contributor on other projects. It is anticipated that a significantly increased effort will be carried out during the next reporting period.

B. SUMMARY OF PRELIMINARY STUDIES

Preliminary studies on the importance of self-focusing of the beam in laser material due to the nonlinear index have been undertaken. Most of the effort here involved a detailed study of the work of G. M. Zverev and V. A. Pashkov.[2] The mathematical derivation of their result for the length of the filamentary damage track as a function of power was verified. A detailed derivation of their results is included as an appendix to this report. The derivation given in the original publication was extremely sketchy. Because of the interest in this work, it is probably useful to have available the more detailed derivation carried out in the appendix. An independent experimental verification of the results of Zverev and Pashkov would be of great interest. In particular, their results on the dependence of the length of the damage track on laser power should be independently verified.

Some preliminary studies of the damage and resultant plasma created at the entrance and exit surfaces of the sample were carried out. In particular, the interaction of the laser beam with the blow-off plasma has been investigated. Theoretically, it is extremely difficult to predict the properties of this plasma. In an extreme case, however,

it is conceivable that the electron density in this plasma could be as high as 10^{20} - 10^{22} cm^{-3}. The electron-plasma frequency in this case would be in the range of 10^{14} - 10^{15} Hz. It has recently been shown in work at HRL and at Princeton that when the laser frequency is close to the electron-plasma frequency, an instability can be excited in the plasma resulting in an anomalously large absorption of the incident radiation. For plasma temperatures of 1 keV the threshold power density for the excitation of this instability is estimated to be about 10^{14} W/cm^2. If this effect takes place at the entrance face of the sample of laser material, the plasma may effectively absorb a significant fraction of the incident power. Further studies of this effect may be needed in order to assess its importance in the present studies. However, it appears at this point that the power densities necessary for the onset of anomalous absorption are several orders of magnitude higher than those encountered in the present experiments.

Studies of the fundamental interaction of electrons with polar optical phonons in the presence of an intense coherent radiation field have continued. A transport equation has been derived for the space and time development of the electron distribution function under the combined action of the electron-phonon interaction and the laser field. This equation differs significantly from the Boltzmann equation used by previous authors. We are attempting to use this equation to verify the results obtained by the previous theoretical investigator by a different but related approach. The connection of this fundamental approach to the actual damage experiments is still very far from complete. Even once the details of the deposition of the laser energy in the material are understood, the nonlinear dynamics of shock formation, heat transfer, etc., in the material will probably be very complicated.

The theoretical work in these areas will continue during the next period. Major emphasis will be given to understanding the beam dynamics and an attempt to explain the experimental results on the shape of the beam profile as a function of incident power. The difference in this behavior between ruby and sapphire leads to the initial guess that the effect depends on the absorption characteristics of the material.

APPENDIX

SELF-FOCUSING THEORY

The theoretical result of G.M. Zverev and V.A. Pashkov[2] on the length of the filamentary damage track as a function of laser power is of considerable interest for these studies. This appendix carries out the mathematical details of this theory. It is included here since the original papers present only a very rudimentary derivation of these results.

The work of Zverev and Pashkov[2], which we refer to as Z-P, is based on the results of S.A. Akhmanov, A.P. Sukhorukov, and R.V. Khokhlov[3] referred to as A-S-K. These authors start from Maxwell's wave equation

$$\underline{\nabla} \times \underline{\nabla} \times \underline{E} + \frac{1}{c^2} \frac{\partial^2 \underline{E}}{\partial t^2} + \frac{4\pi}{c} \frac{\partial^2}{\partial t^2} \left[\underline{P}^{(\ell)} + \underline{P}^{(n\ell)} \right] = 0 \ , \tag{1}$$

for a material with a linear polarization

$$\underline{P}^{(\ell)} = \underline{\underline{\chi}} \ \underline{E} \ , \tag{2}$$

and a nonlinear polarization including fifth order nonlinearity

$$\underline{P}^{(n\ell)} = \underline{\underline{\chi}}^{(3)} \ \underline{E} \ \underline{E} \ \underline{E} + \underline{\underline{\chi}}^{(5)} \ \underline{E} \ \underline{E} \ \underline{E} \ \underline{E} \ \underline{E} \ , \tag{3}$$

where $\underline{\underline{\chi}}$, $\underline{\underline{\chi}}^{(3)}$, $\underline{\underline{\chi}}^{(5)}$ are second, fourth and sixth order tensors, respectively. It is assumed that the nonlinearity is weak so that

$$P^{(n\ell)} / P^{(\ell)} << 1 \ . \tag{4}$$

A transverse wave solution of the form

$$E = \hat{e}\, A(r,z)\, e^{i(\omega t - kz)} \tag{5}$$

is assumed where z is the direction of propagation of the laser beam and r a radial coordinate (i.e., cylindrical geometry). Then

$$-\underline{\nabla} \times \underline{\nabla} \times \underline{E} = \nabla^2 E = -2ik \frac{\partial A}{\partial z} + \nabla_r^2 A - k^2 A + \frac{\partial^2 A}{\partial z^2} \ . \tag{6}$$

In the so-called quasioptical approximation, $\partial^2 A/\partial z^2$ can be neglected relative to the other terms. The wave equation then becomes

$$2ik \frac{\partial A}{\partial z} = \nabla_r^2 A + \frac{n_2}{n_0} |A|^2 k^2 A + \frac{n_4}{n_0} |A|^4 k^2 A \ . \tag{7}$$

Here, it is assumed that k^2 satisfies the linear relation

$$k^2 = \frac{\omega^2}{c^2} \left(1 + 4\pi \frac{1}{3} \mathrm{Tr}\, \chi\right) = \frac{\omega^2}{c^2} n_0 \ , \tag{8}$$

and n_2 and n_4 are proportional to contractions of the tensors $\underline{\underline{\chi}}^{(3)}$ and $\underline{\underline{\chi}}^{(5)}$. The detailed form of this relationship is not important here. It is sufficient to note that this is equivalent to writing the index of refraction in the form

$$n = n_0 + n_2 |E|^2 + n_4 |E|^4 + \ldots \tag{9}$$

For the derivation of Z-P results, the n_4 term can be neglected. Because of the assumption (8), the theory is limited to weak nonlinearity as in (4).

Next the eikonal s is introduced via the substitution

$$A = A_0 e^{-iks} \quad (A_0, s \text{ real}) \quad . \tag{10}$$

Separation of the resulting equation into real and imaginary parts gives

$$\frac{\partial A_0}{\partial z} + \nabla_r A_0 \cdot \nabla_r s + \frac{1}{2} A_0 (\nabla_r^2 s) = 0 \tag{11}$$

$$\frac{2\partial s}{\partial z} + (\nabla_r s)^2 = \frac{n_2}{n_0} A_0^2 + \frac{n_4}{n_0} A_0^4 + \frac{1}{k^2 A_0} \left[\nabla_r^2 A_0 \right] \quad . \tag{12}$$

It is helpful to understand these equations first in the limit of geometrical optics, i.e., $k \to \infty$. Then (11) and (12) reduce to (also neglecting n_4)

$$\frac{2\partial s}{\partial z} + \left(\frac{\partial s}{\partial r} \right)^2 = \frac{n_2}{n_0} A_0^2 \tag{13}$$

$$\frac{\partial (A_0^2)}{\partial z} + \frac{\partial (A_0)^2}{\partial r} \frac{\partial s}{\partial r} + (A_0)^2 \left[\frac{\partial^2 s}{\partial r^2} + \frac{1}{r} \frac{\partial s}{\partial r} \right] = 0 \quad , \tag{14}$$

where the gradients are written out for cylindrical coordinates.

The next step is to look for solutions of the form

$$s = \frac{\beta(z)\, r^2}{2} + \varphi(z) \tag{15}$$

$$A_0^2 = \frac{E_0^2}{f^2(z)} \left(1 - \frac{r^2}{f^2(z)\, r_0^2} \right) . \qquad (16)$$

The boundary conditions at $z = 0$ require

$$\beta(0) = 1/R \quad ; \quad \varphi(0) = 0 \quad ; \quad f(0) = 1 . \qquad (17)$$

Here, R is the radius of curvature of the incident beam; $R < 0$ corresponding to converging incident rays and $R > 0$ corresponding to diverging incident rays. The condition $f(0) = 1$ implies an incident intensity distribution

$$A_0^2(0, r) = E_0^2(1 - r^2/r_0^2) . \qquad (18)$$

This ansatz is physically reasonable since the surfaces of constant phase are $k(z+s) = \omega t$ or $(z + \beta r^2/2) = c/n_0\, t$, which for $\beta > 0$ have the correct behavior to provide rays focused toward the z-axis. Making the above substitution into eq. (12), we obtain

$$\frac{2E_0^2}{f^2} \left(\beta - \frac{f'}{f} \right) = 0 . \qquad (19)$$

Thus, if we choose

$$\beta = f'/f , \qquad (20)$$

this is automatically satisfied. Substitution of (15) and (16) along with (18) into (15) gives

$$r^2 \frac{f''}{f} + 2\varphi' = \frac{n_2}{n_0} \frac{E_0^2}{f^2} \left(1 - \frac{r^2}{r_0^2 f^2} \right) . \qquad (21)$$

Since f and φ must be functions of z alone, it follows from (21) that

$$\varphi' = \frac{n_2}{2n_0} \frac{E_0^2}{f^2} , \tag{22}$$

and

$$f'' = \frac{-n_2}{n_0} \frac{E_0^2}{f^3 r_0^2} . \tag{23}$$

Multiply both sides of (23) by f' to obtain

$$\frac{1}{2} \frac{d}{dz} (f')^2 = \frac{-n_2}{n_0} \frac{E_0^2}{f^3 r_0^2} f' , \tag{24}$$

which can be integrated to give

$$\left(\frac{df}{dz}\right)^2 = \frac{n_2}{n_0} \frac{E_0^2}{r_0^2 f^2} + C . \tag{25}$$

Applying the boundary conditions at z = 0 ,

$$\beta(0)^2 = \frac{f'(0)^2}{f(0)^2} = \frac{n_2}{n_0} \frac{E_0^2}{r_0^2} + C = \frac{1}{R^2} \tag{26}$$

$$C = \frac{1}{R^2} - \frac{n_2 E_0^2}{n_0 r_0^2} . \tag{27}$$

Multiply (25) by f^2 to obtain

$$\frac{1}{2}\frac{d}{dz} f^2 = \pm \sqrt{\frac{n_2}{n_0}\frac{E_0^2}{r_0^2} + Cf^2} \quad ,$$

which can be integrated directly to give

$$\pm \sqrt{\frac{n_2}{n_0}\frac{E_0^2}{r_0^2} + Cf^2} = C(z + \text{const}) \quad .$$

At $z = 0$, we determine

$$\text{const} = \pm \frac{1}{c}\sqrt{\frac{n_2}{n_0}\frac{E_0^2}{r_0^2} + C} = \pm \frac{1}{C}\frac{1}{R} \quad .$$

Thus, we have the solution

$$f^2 = \left(\frac{1}{R^2} - \frac{n_2 E_0^2}{n_0 r_0^2}\right) z^2 + \frac{2z}{R} + 1 \quad . \tag{28}$$

From this we can determine φ using (22) and (17).

This solution determines two focal points at which $f(z) = 0$, which implies $A_0^2(z, 0) = \infty$. From (28) we obtain the two roots

$$\frac{1}{z_{f_2}} = \frac{1}{R_{n\ell}} - \frac{1}{R} \quad , \tag{29}$$

where

$$R_{n\ell} = r_0 \sqrt{\frac{n_0}{n_2 E_0^2}} \quad , \tag{30}$$

and

$$\frac{1}{z_{f_2}} = -\frac{1}{R} - \frac{1}{R_{n\ell}} \quad . \tag{31}$$

The distance $R_{n\ell}$ is that over which a light beam with a plane phase front ($R \to \infty$) and an intensity distribution given by (18) would be self-focused in a nonlinear medium. For a converging beam ($R < 0$), the focal length z_{f_1} decreases in a nonlinear medium with $n_2 > 0$. An initially diverging beam becomes self-focused at z_{f_1} provided $R \leq R_{n\ell}$. The second focus z_{f_2} exists only if $R < 0$ (converging) and in this case $z_{f_2} > z_{f_1}$ since $R < -R_{n\ell}$.

Next we include diffraction effects, i.e., the last term on the right-hand side of (12), following A-S-K but neglecting the n_4 term which they include. Here, a gaussian intensity distribution is assumed

$$A_0^2(r, z) = \frac{E_0^2}{f^2(z)} \exp\left(\frac{-r^2}{r_0^2 f^2(z)}\right) , \tag{32}$$

which reduces to (16) when $r^2 << r_0^2 f^2$. In place of (21) we now obtain

$$r^2 \frac{f''}{f} + 2\phi' = \frac{n_2}{n_0} \frac{E_0^2}{f^2} \left(1 - \frac{r^2}{r_0^2 f^2}\right) + \frac{1}{k^2} \left[\frac{-2}{f^2 r_0^2} + \frac{r^2}{f^4 r_0^4}\right] , \tag{33}$$

where we have expanded $A_0^2(r,z)$ to terms proportional to $r^2/(r_0^2 f^2)$. Proceeding as before, we now find

$$2\varphi' = \frac{n_2 E_0^2}{n_0 f^2} - \frac{2}{k^2 f^2 r_0^2} , \tag{34}$$

and

$$f'' = - \frac{n_2}{n_0} \frac{E_0^2}{r_0^2 f^3} + \frac{1}{k^2 r_0^4 f^3} . \tag{35}$$

Thus, we can write using (30)

$$\frac{d^2 f}{dz^2} = - \frac{1}{R_{n\ell}^2 f^3} + \frac{1}{R_d^2 f^3} , \tag{36}$$

where

$$R_d = k r_0^2 . \tag{37}$$

Equation (36) is the starting point for the work of Z-P. In this paper f is denoted as δ. This can be integrated as in the geometrical optics case to give

$$\left(\frac{df}{dz}\right)^2 = \frac{1}{f^2}\left(\frac{1}{R_{n\ell}^2} - \frac{1}{R_d^2}\right) + C , \tag{38}$$

where

$$C = \frac{1}{R^2} - \frac{1}{R_{n\ell}^2} + \frac{1}{R_d^2} \quad . \tag{39}$$

Define:

$$\frac{1}{R_{dn}^2} \equiv \frac{1}{R_d^2} - \frac{1}{R_{n\ell}^2} \tag{40}$$

$$\left(\frac{df}{dz}\right)^2 = -\frac{1}{f^2 R_{dn}^2} + \frac{1}{R^2} + \frac{1}{R_{dn}^2} \quad . \tag{41}$$

We restrict our considerations now to beam powers less than critical, i.e., to $R_{n\ell} > R_d$. In this case, self-focusing leads to a decrease of the focal spot diameter compared to the diffraction diameter d_0 . The minimum diameter of the beam d is determined from setting df/dz = 0:

$$\frac{1}{f^2} = 1 + \frac{R_{dn}^2}{R^2} \approx \frac{R_{dn}^2}{R^2} \quad . \tag{42}$$

It follows from (40) that

$$R_{dn}^2 = \frac{R_{n\ell}^2}{\frac{R_{n\ell}^2}{R_d^2} - 1} = \frac{R_{n\ell}^2}{\left(\frac{P_{cr}}{P} - 1\right)} \quad , \tag{43}$$

where the critical power is defined by $R_{n\ell}^2 = R_d^2$, i.e.,

$$\frac{r_0^2 n_0}{E_0^2 n_2} = k^2 r_0^4 \tag{44}$$

$$P_{cr} = \pi r_0^2 \frac{E_0^2 c}{8\pi} = \frac{\pi r_0^2}{8\pi n_2} \frac{c}{k^2 r_0^2} = \frac{\lambda_0^2 c}{32\pi^2 n_2} , \tag{45}$$

where λ_0 is the linearly determined wave length $n_0 \lambda_0 = 2\pi/k$. Therefore, from (43) we have

$$d = d_0 (1 - P/P_{cr})^{1/2} , \tag{46}$$

where $d = 2f r_0$ is the focal spot diameter and

$$d_0 = 2r_0 \frac{R}{R_{n\ell}} \sqrt{\frac{P_{cr}}{P}} = 2r_0 \frac{R}{R_d} = \frac{R}{\pi} \frac{\lambda_0}{r_0 n_0} , \tag{47}$$

since $\sqrt{P_{cr}/P} = R_{n\ell}/R_d$. The quantity d_0 is the diffraction-limited spot diameter. (Note the beam diameter a of Z-P is related to r_0 by $a = 2r_0$.)

As the radiation power increases, the diameter d decreases until the power density at the focus reaches the threshold value I_{thr} necessary for damage to the material. Now from

$$I_{thr} = P_{thr}/(\pi d^2/r) = \frac{4 P_{thr}}{\pi d_0^2 \left[1 - \frac{P_{thr}}{P_{cr}}\right]} . \tag{48}$$

solving for P_{thr} we find

Z-P (9)
$$P_{thr} = \frac{(\pi/4)\, d_0^{\,2}\, I_{thr}}{1 + (\pi/4)\, d_0^{\,2}\, I_{thr}/P_{cr}} \quad . \tag{49}$$

The formula in Z-P has $\pi/4$ replaced by 1, which is incorrect but a minor difference.

If $(\pi/4)d_0^{\,2}\, I_{thr}/P_{cr} >> 1$, then $P_{thr} \approx P_{cr}$ and d is much less than d_0 as a result of self-focusing.

The length of the filamentary damage track is determined as the difference between the focal distance of the lens in the sample z_f, where the damage begins, and the minimum length of self-focusing z_{sf} which determines the position of the end of the filament. We are now considering the case of beam powers above the critical value so $R_{n\ell} < R_d$ and $R_{dn}^{\,2} < 0$ [see (40)]. In this case we can write (41) as

$$\left(\frac{df}{dz}\right)^2 = \frac{1}{f^2 R_{nd}^{\,2}} + \frac{1}{R^2} - \frac{1}{R_{nd}^{\,2}} \quad , \tag{50}$$

where

$$\frac{1}{R_{nd}^{\,2}} = \frac{1}{R_{n\ell}^{\,2}} - \frac{1}{R_d^{\,2}} \quad , \tag{51}$$

so

$$R_{nd} = R_{n\ell}\,(1 - P_{cr}/P)^{-1/2} \quad . \tag{52}$$

Note that this equation has the same form as (25) in the geometrical optics case but with $R_{n\ell}^2$ replaced by R_{nd}^2 [see also (27)]. Thus, we can directly use (29) to write for the focal distance

$$\frac{1}{z_{sf}} = \frac{1}{R_{nd}} + \frac{1}{|R|} \tag{53}$$

for $R < 0$. The length of the filament is for $|R| << R_{nd}$

$$L = z_f - z_{sf} = \frac{R^2}{|R| + R_{nd}} \simeq \frac{R^2}{R_{nd}} = \frac{R^2}{R_{nd}} \left(1 - \frac{P_{cr}}{P}\right)^{1/2} \tag{54}$$

$$= \frac{R^2}{P^{1/2} R_{n\ell}} (P - P_{cr})^{1/2} \tag{55}$$

$$= \frac{R^2}{P_{cr}^{1/2} R_d} (P - P_{cr})^{1/2} . \tag{56}$$

Now

$$P_{cr} R_d^2 = \frac{\lambda_0^2 c}{32\pi^2 n_2} k^2 r_0^4 = \frac{n_0}{8} \frac{c^2 r_0^4}{n_2} . \tag{57}$$

So

$$\text{Z-P (12)} \qquad L = 4\sqrt{2} \sqrt{\frac{n_2}{c n_0}} \frac{R^2}{(2r_0)} (P - P_{cr})^{1/2} , \tag{58}$$

which is the central result of Z-P.

Z-P convert this into an approximate result by noting that z_{sf} determines the position of zero spot size, whereas it is physically clear and follows from eq. (49) that damage occurs for $d > 0$. The expression for L vanishes for $P = P_{cr} > P_{thr}$, whereas we expect L to vanish for $P = P_{thr}$. This is corrected by Z-P by making the approximate replacement of P_{cr} by P_{thr} in (58).

Z-P (13) $$L \approx 4\sqrt{2}\sqrt{\frac{n_2}{cn_0}}\frac{R^2}{(2r_0)}(P - P_{thr})^{1/2} . \qquad (59)$$

REFERENCES

1. I. M. Winer, Applied Optics 5, 1437 (1966).

2. G. M. Zverev and V. A. Pashkov, Soviet Physics, JETP 30, 616 (1970).

3. S. A. Akhmanov, A. P. Sukhorukov, and R. V. Khokhlov, Soviet Physics, JETP 23, 1025 (1966).

UNCLASSIFIED
Security Classification

DOCUMENT CONTROL DATA - R&D

(Security classification of title, body of abstract and indexing annotation must be entered when the overall report is classified)

1. ORIGINATING ACTIVITY *(Corporate author)*
Hughes Research Laboratories
3011 Malibu Canyon Road
Malibu, California 90265

2a. REPORT SECURITY CLASSIFICATION
Unclassified

2b. GROUP

3. REPORT TITLE
DAMAGE THRESHOLD STUDIES IN LASER CRYSTALS:
BEAM INTENSITY PROFILE AND SELF-FOCUSING

4. DESCRIPTIVE NOTES *(Type of report and inclusive dates)*
Scientific. Interim.

5. AUTHOR(S) *(First name, middle initial, last name)*
Concetto R. Giuliano Robert W. Hellwarth
Donald F. DuBois Gerald R. Rickel

6. REPORT DATE	7a. TOTAL NO. OF PAGES	7b. NO. OF REFS
January 1971	61	3

8a. CONTRACT OR GRANT NO.	9a. ORIGINATOR'S REPORT NUMBER(S)
F19628-69-C-0277	Semi-Annual Report No. 3
b. PROJECT, TASK, WORK UNIT NOS. Project No. 8693	
c. DOD ELEMENT 61101D	9b. OTHER REPORT NO(S) *(Any other numbers that may be assigned this report)* AFCRL-71-0064
d. DOD SUBELEMENT N/A	

10. DISTRIBUTION STATEMENT
1- This document has been approved for public release and sale; its distribution is unlimited.

11. SUPPLEMENTARY NOTES	12. SPONSORING MILITARY ACTIVITY
TECH, OTHER	Air Force Cambridge Research Laboratories (OP) L.G. Hanscom Field Bedford, Massachusetts 01730

13. ABSTRACT

In this report the results of a number of experiments are presented which were aimed at detailed characterization of the spatial profile of the laser beam both before and after amplification. It was found that the beam profile in the near field of the laser deviates significantly from a gaussian, but that in the far field it is very close to a gaussian. It was also found that while the amplifier does not contribute to significant beam distortion, it acts as a negative lens whose focal length decreases with increased optical pumping. The purpose of these continuing measurements is to have a close measurement of the size and location of the focused beam waist. Based on these measurements, revised values of previous damage thresholds are presented as well as the results of measurements of damage threshold as a function of lens focal length. In other experiments, the time evolution of the damage tracks in ruby and sapphire was studied using a fast streaking camera. It was found that the point on the damage filament furthest from the laser forms first, and the track evolves in an upstream direction. Beam profile measurements inside ruby samples show a severe power dependent beam distortion which begins to appear at powers well below the damage threshold. This breaking up of the beam is not observed in sapphire. It is possible that this breaking up of the beam in ruby is connected with the absorption at 6943 Å. Because of the importance of self-focusing considerations in damage studies, a detailed derivation of theoretical results reported recently by other workers is presented as an appendix.

DD FORM 1 NOV 65 1473

UNCLASSIFIED
Security Classification

14. KEY WORDS	LINK A		LINK B		LINK C	
	ROLE	WT	ROLE	WT	ROLE	WT
Bulk Damage						
Damage Thresholds						
Lasers						
Ruby						
Sapphire						
Self-Focusing						
Streak Camera Experiments						
Gaussian Beams						
Amplifier Lensing						
Beam Profile Measurements						
Beam Distortion						